Liquid Crystals
Publication details, including instructions for authors and subscription information:
http://www.informaworld.com/smpp/title~content=t713926090

Magnetic and electric field induced periodic deformations in planar oriented nematics

U. D. Kini

Online publication date: 06 August 2010

To cite this Article Kini, U. D.(1998) 'Magnetic and electric field induced periodic deformations in planar oriented nematics', Liquid Crystals, 24: 2, 177 — 199
To link to this Article: DOI: 10.1080/026782998207352
URL: http://dx.doi.org/10.1080/026782998207352

LIQUID CRYSTALS, 1998, VOL. 24, NO. 2, 177–199

Magnetic and electric field induced periodic deformations in planar oriented nematics

by U. D. KINI
Raman Research Institute, Bangalore—560 080, India

(*Received 23 July 1997; accepted 6 August 1997*)

Using the continuum theory in the linear perturbation limit, the formation of static periodic distortions (PD) is studied in a planar nematic sample under the action of crossed electric (**E**) and magnetic (**H**) fields. In a nematic dielectric with positive dielectric and diamagnetic anisotropies ($\varepsilon_A > 0$, $\chi_A > 0$), the wave vector of **H** induced PD depends on the tilt of **H** in a plane normal to the initial director orientation $\mathbf{n}_o$ when **E** is in the sample plane; change of magnetic tilt may cause discontinuous changes in the wave vector. Similar results are obtained when electrical conductivity is taken into account with hydrodynamic effects being assumed absent. Calculations are extended to a study of PD in nematics with high elastic anisotropy for different signs of ε_A and χ_A. When such materials have susceptibility anisotropies of opposite sign, change in magnetic tilt may cause 're-entrant' appearances of distortions. When anchoring is weak enough, the saddle–splay elastic constant K_{24} can influence the domain of existence of PD. Possible effects of flexoelectricity as well as results for cylindrical geometry are qualitatively discussed.

1. Introduction

The continuum theory [1–4] satisfactorily explains many effects arising from the action of external magnetic (**H**) and electric (**E**) fields on nematic samples. The nematic director (**n**) can be uniformly oriented (along $\mathbf{n}_o$, say) in a sample by appropriate treatment of the bounding planes; the surface treatment also determines the director anchoring strength [5]. The planar ($\mathbf{n}_o$ parallel to the sample planes) and the homeotropic ($\mathbf{n}_o$ normal to the sample planes) alignments are commonly used. For simplicity, the *rigid anchoring* hypothesis is frequently employed in theoretical calculations. **H** or **E** either stabilizes or destabilizes $\mathbf{n}_o$ depending upon the sign of the relevant susceptibility anisotropy of the material and the direction of the field relative to $\mathbf{n}_o$. The effect of simultaneous application of a stabilizing and a destabilizing field along symmetry directions (*crossed field configuration*) is also studied.

The application of **H** normal to $\mathbf{n}_o$ leads to the aperiodic or homogeneous distortion (HD) above a well defined Fréedericksz threshold in materials with moderate elastic anisotropy; the optical detection of HD helps in the evaluation of the splay (K_1), twist (K_2) and bend (K_3) curvature (bulk) elastic constants if χ_A is known. In nematics with high elastic anisotropy (e.g. high molecular weight nematic or nematic close to the nematic–smectic A transition), the distortion above a magnetic threshold may be periodic (PD) [6, 7]. It can be shown [6, 8] that when the elastic anisotropy is high enough, the PD threshold is lower than the HD threshold. Theoretical interpretations of the effects of **H** are generally straightforward as the field is not appreciably modified by the medium even in the presence of spatial gradients of **n**.

In contrast to magnetic effects, the effects of **E** are far more diverse, complex and interesting since **E** inside the medium is strongly affected by director gradients [9], flexoelectric polarization (**P**) [10], electrical conductivity, etc. A number of studies have been reported on planar oriented samples [3, 4]. As the coupling between **P** and **E** is linear, the influence of **P** can be greatly reduced by using an a.c. field of sufficiently high frequency. Under the action of a d.c. field, however, PD occurs even in materials with low elastic anisotropy due to flexoelectricity [11]. The variation of the principal dielectric constants caused by an increase of the electric frequency also leads to PD in some nematics [12]. When different director anchoring strengths are imparted to the sample planes, even the magnitude of the d.c. Fréedericksz threshold changes with the voltage polarity [13]. An impure nematic has low electrical conductivity whose anisotropy can be controlled by different methods [3]. When such a material is subjected to **E**, a variety of convective electrohydrodynamic instabilities set in. Different mechanisms that cause these instabilities have been theoretically identified [3, 4, 14]

taking explicit account of electrical conductivity, charge injection, etc. Though dynamic effects generally accompany the presence of conductivity, theoretical attempts have been made to study the effect of conductivity on static HD [9]. It should be interesting to extend these studies to include static PD.

A number of effects have also been observed in homeotropically aligned nematic samples with **E** impressed in the sample plane. A d.c. field causes thresholdless HD due to flexoelectricity in a weakly anchored sample [15]. With strong anchoring, an a.c. field produces a first order Fréedericksz transition [16, 17] in a material (such as 5CB) with positive susceptibility anisotropies [18]. With an additional stabilizing **H**, PD appears above a well defined threshold [17]. A nonlinear [19] and a linear [20] mathematical model have been proposed to explain the electric PD threshold as a dielectric effect. The analysis of [20] is mathematically simpler and gives an insight into the instability mechanism which comprises mainly the additional destabilizing torques resulting from periodic electric perturbations. Results for rigid anchoring [20] are in qualitative agreement with the findings of reference [17].

The model of reference [20] has been extended [21] to the study of PD in homeotropic samples of materials (such as M1 [22] and CCH–7 [23]) having susceptibility anisotropies of opposite signs, with **E** and **H** acting in the sample plane; depending upon the material parameters, one can study either the electric or the magnetic PD threshold. The PD threshold as well as the periodicity wave vector depend strongly on the angle between **H** and **E** [21]. The pretilt of $\mathbf{n}_o$ away from the homeotropic suppresses PD [24] so that only HD sets in under the action of the destabilizing field. A transition from PD to HD occurs due to the variation of field strengths as well as that of the angle between the fields; a variety of phase diagrams now results. This transition is of second order for rigid anchoring [21], but becomes discontinuous when the director is weakly anchored [25].

Close mathematical similarity exists between the governing equations for homeotropic and planar configurations [1–4, 17]. It is, therefore, possible that PD of the kind studied in [20, 21, 24, 25] may also be obtained as a solution for planar $\mathbf{n}_o$ in nematics with moderate elastic anisotropy when **E** is impressed in the sample plane. This provides the motivation to study the initial planar orientation. So far, PD induced by elastic anisotropy has been studied only in high molecular weight materials with positive susceptibility anisotropies [6, 8]. Such materials with opposite signs of susceptibility anisotropies may also exist. The previously developed mathematical models [8] can be extended to the study of PD in such cases, especially with **E** impressed along different symmetry directions with respect to $\mathbf{n}_o$. It should be interesting to compare the phase diagrams obtained for different materials.

Work referenced above concerns flat nematic samples and defectless deformations involving bulk curvature elastic constants. With the advent of polymer dispersed liquid crystal (PDLC) displays (see [26] for a review), a number of studies on singular nematic configurations confined to cylindrical cavities have led to the determination of the (saddle–splay) surface elastic constant K_{24} of some nematics [27]. The effect of K_{24} on PD may be considerable even in flat, sufficiently thin samples [28]. It should be interesting to study the influence of K_{24} on PD for different field configurations in a flat sample when the director anchoring is weak.

With the above motivation, the governing equations are set up along with general boundary conditions in § 2. In § 3, results are presented for different deformations under the rigid anchoring hypothesis with **E** acting in the sample plane. These calculations are generalized to the finite anchoring case in § 4 with a brief summary of possible effects of flexoelectricity. In § 5, PD caused by high elastic anisotropy is studied for different material types with **E** impressed normal to the sample planes. These results are contrasted with those of § 6 obtained for **E** acting in the sample plane normal to $\mathbf{n}_o$. Section 7 summarizes the main results of this work and indicates possible extensions to the study of PD in cylindrical geometry. The Appendix contains a purely formal derivation of the PD threshold in the presence of electrical conductivity.

2. Governing equations; boundary conditions for E parallel to the plates

The nematic insulator is initially aligned along x with $\mathbf{n}_o=(1,0,0)$ between parallel glass plates $z=\pm h$ and flat electrodes at $x=\pm g$ such that the electrode gap $(2g)$ is large compared with the sample thickness $(2h)$, with the region of interest being close to $x=0$. A potential difference V_X is impressed between the electrodes. The magnetic intensity **H** is either along x,

$$\mathbf{H}_\parallel=(H_\parallel,0,0)$$

or in the yz plane,

$$\mathbf{H}_\perp=(0,H_\perp C\alpha,H_\perp S\alpha);\quad C\alpha=\cos\alpha;\quad S\alpha=\sin\alpha.$$

When $\alpha=\pi/2$, $\mathbf{H}_\perp$ is along z; when α vanishes, $\mathbf{H}_\perp$ is along y. These α values correspond to symmetry directions for planar alignment. Inside the sample, the unperturbed electric field is

$$\mathbf{E}_o=(E_{xo},0,0);\quad E_{xo}=V_X/2g.$$

When perturbations are imposed on $\mathbf{n}_o$, the electric field also becomes modified,

$$\mathbf{n}=(C_\theta C_\phi,S_\phi,S_\theta C_\phi);\quad \mathbf{E}=\mathbf{E}_o+\mathbf{E}';\quad \mathbf{E}'=-\nabla\psi \quad (1)$$

where θ, ϕ and ψ are functions of x, y and z. Maxwell's curl equation has been employed to express the electric perturbation as the gradient of a scalar potential, implicitly making the assumption that the nematic is an insulator. The perturbations and their derivatives are assumed to be small so that only terms up to linear order are retained in the governing equations. For constant potential difference between electrodes, the total free energy F of the sample is

$$F=\int_A W^{\Lambda}\,\mathrm{d}\Lambda + A\,W_S(z=h) + A\,W'_S(z=-h);$$

$$W^{\Lambda}=\frac{K_1}{2}(\phi_{,y}^2+\theta_{,z}^2)+\frac{K_2}{2}(\phi_{,z}^2+\theta_{,y}^2)+\frac{K_3}{2}(\phi_{,x}^2+\theta_{,x}^2)$$
$$+(K_1-K_{24})\phi_{,y}\theta_{,z}+(K_{24}-K_2)\phi_{,z}\theta_{,y}$$
$$-\frac{\varepsilon_{\parallel}}{8\pi}\psi_{,x}^2-\frac{\varepsilon_{\perp}}{8\pi}(\psi_{,y}^2+\psi_{,z}^2)+f_M+f_E+f_F;$$

$$f_F=0;\quad f_E=\frac{\varepsilon_A E_{xo}^2}{8\pi}(\theta^2+\phi^2)+\frac{\varepsilon_A E_{xo}}{4\pi}(\phi\psi_{,y}+\theta\psi_{,z});$$

$$f_M=\frac{\chi_A H_{\parallel}^2}{2}(\theta^2+\phi^2)\ \text{if}\ H_{\perp}=0\ \text{or}$$

$$f_M=-\frac{\chi_A H_{\perp}^2}{2}(S\alpha\theta+C\alpha\phi)^2\ \text{if}\ H_{\parallel}=0;$$

$$W_S=\frac{B_\phi}{2}\phi^2+\frac{B_\theta}{2}\theta^2;\quad W'_S=\frac{B'_\phi}{2}\phi^2+\frac{B'_\theta}{2}\theta^2 \qquad (2)$$

where Λ is the sample volume, W^{Λ} the volume free energy density [27], A the area of either plate, W_S and W'_S the surface free energy densities at the two plates in the Rapini–Papoular form [5] and a subscripted comma denotes partial (or ordinary) differentiation; $\varepsilon_A=\varepsilon_{\parallel}-\varepsilon_{\perp}$ where $\varepsilon_{\parallel}$ and $\varepsilon_{\perp}$ are, respectively, the dielectric constants parallel to and normal to $\mathbf{n}_o$; B_θ, B'_θ are polar anchoring strengths at $z=\pm h$, respectively; B_ϕ and B'_ϕ are the corresponding azimuthal anchoring strengths. While only the polar anchoring strength is relevant for homeotropic alignment [25], both anchoring strengths appear in the present case. Terms of zero and first order have been dropped from W^{Λ} as they seem to be inoperative. Terms corresponding to flexoelectricity are omitted for the present ($f_F=0$); this may be a meaningful assumption if V_X is time varying with a sufficiently high frequency. However, possible effects of flexoelectricity are briefly discussed in § 4.3.

Of the three perturbations, θ and ϕ are the angular variations of the unit director. The governing equations are derived by minimizing F with respect to each of the three perturbations. While studying a virtual variation of one variable (say, ψ), the other two are held fixed; then, Maxwell's divergence equation results [29]:

$$\varepsilon_A E_{xo}(\phi_{,y}+\theta_{,z})-\varepsilon_{\parallel}\psi_{,xx}-\varepsilon_{\perp}(\psi_{,yy}+\psi_{,zz})+A_F=0;$$
$$A_F=0. \qquad (3)$$

The modifications of $\mathbf{E}$ are connected to derivatives of θ and ϕ. The flexoelectric term A_F is neglected for the present. The two independent components of the torque equation result from a variation of F with respect to θ and ϕ:

$$K_3\theta_{,xx}+K_2\theta_{,yy}+K_1\theta_{,zz}+a_\theta\theta+(K_1-K_2)\phi_{,yz}$$
$$+a_\phi\phi+U_\theta=0 \qquad (4)$$

$$K_3\phi_{,xx}+K_1\phi_{,yy}+K_2\phi_{,zz}+b_\phi\phi+(K_1-K_2)\theta_{,yz}$$
$$+b_\theta\theta+U_\phi=0 \qquad (5)$$

$$a_\theta=\chi_A H_{\perp}^2 S^2\alpha,\quad a_\phi=b_\theta=\chi_A H_{\perp}^2 S\alpha C\alpha,\quad b_\phi=\chi_A H_{\perp}^2 C^2\alpha\ \text{or}$$
$$a_\theta=b_\phi=-\chi_A H_{\parallel}^2,\quad a_\phi=b_\theta=0;$$

$$U_\theta=-\frac{\varepsilon_A E_{xo}}{4\pi}\psi_{,z}-\frac{\varepsilon_A E_{xo}^2}{4\pi}\theta;$$

$$U_\phi=-\frac{\varepsilon_A E_{xo}}{4\pi}\psi_{,y}-\frac{\varepsilon_A E_{xo}^2}{4\pi}\phi. \qquad (6)$$

The volume torque does not depend on K_{24} which appears only in the surface elastic torque relevant to the boundary conditions:

$$\frac{\partial W^{\Lambda}}{\partial\theta_{,z}}+B_\theta\theta=0;\quad \frac{\partial W^{\Lambda}}{\partial\phi_{,z}}+B_\phi\phi=0\ \text{at}\ z=h;$$

$$\frac{\partial W^{\Lambda}}{\partial\theta_{,z}}-B'_\theta\theta=0;\quad \frac{\partial W^{\Lambda}}{\partial\phi_{,z}}-B'_\phi\phi=0\ \text{at}\ z=-h;$$

$$\frac{\partial W^{\Lambda}}{\partial\theta_{,z}}=K_1\theta_{,z}+(K_1-K_{24})\phi_{,y}+\tau_\theta;\quad \tau_\theta=0$$

$$\frac{\partial W^{\Lambda}}{\partial\phi_{,z}}=K_2\phi_{,z}-(K_2-K_{24})\theta_{,y}. \qquad (7)$$

The term τ_θ is useful for including flexoelectric contributions. Clearly, θ and ϕ will not vanish at the boundaries as is true for rigid anchoring. The third boundary condition is related to ψ. While $\mathbf{E}$ inside the glass (isotropic dielectric) plates is along x, $\mathbf{E}$ inside the nematic, from equation (1), is perturbed. Inside glass, the electric induction $\mathbf{D}$ is also directed along x so that the normal component (D_z) vanishes. Continuity of D_z at the interfaces between the nematic (anisotropic dielectric) and glass implies [29] that

$$\varepsilon_A E_{xo}\theta-\varepsilon_{\perp}\psi_{,z}+\lambda_D=0\ \text{at}\ z=\pm h;\quad \lambda_D=0. \qquad (8)$$

The flexoelectric contribution (λ_D) is ignored at present. As done earlier ([20, 24, 25]; see also note 26 in [21]), the additional condition of continuity of tangential components of $\mathbf{E}$ at the interfaces is not explicitly imposed.

The solution of equations (3)–(5) with (7) and (8) generally reduces to that of an eigenvalue problem. Depending upon the attributes of the distortion, the required subset of terms from equations (3)–(8) is chosen. **H** is also selected for a given configuration such that it either stabilizes or destabilizes $\mathbf{n}_o$. Without loss of generality, E_{xo} (or V_X) can be assumed to be positive because the transformation

$$E_{xo} \rightarrow -E_{xo}, \quad \psi \rightarrow -\psi$$

leaves equations (3)–(8) unaltered. In general, four different solutions can be studied:

Homogeneous deformation HD: perturbations vary with z.
X Mode: PD with wave vector along x; perturbations depend on x and z.
Y Mode: PD with wave vector along y; perturbations vary with y and z.
XY Mode: PD with wave vector lying in the xy plane (plane of the sample); perturbations depend on all three coordinates.

The action of K_{24} in the surface torques (7) is opposed to that of K_2 or K_1. In addition, K_{24} appears in equation (7) only when θ and ϕ depend on y. Hence, K_{24} affects only the Y and XY Modes. An estimate of the magnitude of K_{24} is obtained by restricting the quadratic form representing the elastic free energy density in $W^{\wedge}$ to be definitely positive. Apart from the four elastic constants being definitely positive, one must have

$$K_{24} < 2K_1; \quad K_{24} < 2K_2.$$

If $K_1 > K_2$ (which is usually the case), the second restriction is taken; in the opposite case, the former is assumed. In either case, the maximum value of K_{24} is of the same order of magnitude as K_1 or K_2.

In reality, the anchoring strengths $\sim 10^{-4}$ to 10^{-2} erg cm^{-2} [5]. The strong anchoring limit is particularly interesting as it yields analytical solutions in many cases. In this limit, the magnitude of the product of anchoring strength and director perturbation in equations (7) is large compared with the derivative terms representing the elastic surface torque, so that the magnitudes of θ and ϕ at the boundaries are small at threshold in spite of a deformation in the bulk. In the extreme case of rigid anchoring, both perturbations will vanish at the boundaries. Then, equations (7) and (8) reduce to

$$\theta = 0; \quad \phi = 0; \quad \psi_{,z} = 0 \text{ at } z = \pm h. \tag{9}$$

For moderate fields, the PD wavelength at threshold is $\sim$ the sample thickness. Hence, the surface torque $\sim K\theta/h$ where K is an average elastic constant. This should be small compared with $B\theta$ for strong anchoring. In other words, the dimensionless quantity $\sigma = Bh/K \gg 1$. With $B \sim 10^{-2}$ erg cm^{-2}, $h \sim 10^{-2}$ cm and $K \sim 10^{-6}$ dyne, $\sigma \sim 10^2$; this would correspond to strong anchoring. On the other hand, $\sigma \sim 1$ if $h \sim 10^{-4}$ cm (very thin sample). Then, the bulk elastic torque may cause non-vanishing θ and ϕ at the boundaries; the influence of K_{24} may also be felt on the distortion. Thus, sample thickness is a relevant parameter in thin samples with weak anchoring.

The general case of different anchoring strengths at the two boundaries introduces four parameters into equations (7). For simplicity, we assume that the corresponding anchoring strengths at the two plates are equal:

$$B'_\theta = B_\theta; \quad B'_\phi = B_\phi.$$

With this, it is possible to study uncoupled solutions with definite spatial symmetry relative to $z = 0$ in many situations.

3. Material with positive ε_A and χ_A

The material chosen is 5CB [18] with the material parameters at 28°C:

$$(K_1, K_2, K_3) = (5{\cdot}21, 2{\cdot}71, 6{\cdot}67) \times 10^{-7} \text{ dyne};$$
$$\chi_A = 1{\cdot}1 \times 10^{-7} \text{ emu};$$
$$(\varepsilon_\parallel, \varepsilon_\perp) = (17{\cdot}86, 7{\cdot}25); \quad \varepsilon_A = 10{\cdot}61. \tag{10}$$

As $\mathbf{E}_o$ stabilizes $\mathbf{n}_o$, it is natural to consider $\mathbf{H}_\perp$ with $H_\parallel = 0$. The anchoring is assumed to be rigid.

3.1. *Results for rigid anchoring with $\alpha = \pi/2$*

Now, equations (3)–(8) assume a particularly simple form. We start with HD; with dependence on z, ϕ gets decoupled from θ and ψ in equation (5). Due to equation (9), ϕ damps out in the sample as $\mathbf{H}_\perp$ acts along z and ϕ is in the xy plane. Equations (3) and (4) lead to a second order differential equation in θ supporting two uncoupled solutions. We choose the solution with θ symmetric (and ψ antisymmetric). With the *ansatz* $\theta = \theta_M \cos(qz/h)$, it is required to find the lowest $H_\perp$ at which θ_M is non-zero. This yields the splay Fréedericksz threshold H_F,

$$H_F = \left[(q^2 + \omega_E) \frac{K_1}{\chi_A h^2} \right]^{1/2}; \quad \omega_E = \frac{\varepsilon_A \varepsilon_\parallel h^2 E_{xo}^2}{4\pi K_1 \varepsilon_\perp}; \quad q = \frac{\pi}{2}. \tag{11}$$

Clearly, the above is an eigenvalue problem. At HD threshold, we only know that θ_M is non-zero but its value is not known. The factor $\varepsilon_\parallel/\varepsilon_\perp$ appears in ω_E as a consequence of the torque due to $\psi_{,z}$ in equation (4).

The X Mode again does not involve ϕ. Equations (3) and (4) now support two uncoupled solutions:

X Mode SOLUTION 1: θ is symmetric and ψ antisymmetric.

X Mode SOLUTION 2: θ is antisymmetric and ψ symmetric.

SOLUTION 1 has the same spatial symmetries as HD and the X Mode becomes an extension or generalization of HD. The *ansatz* for a closed solution is

$$(\theta, \psi) = [\theta_M \cos(qz/h) \sin(q_x x), \psi_M \sin(qz/h) \sin(q_x x)]$$

where q_x, the wave vector of periodicity along x, depends on material parameters, field strengths and sample thickness. Substituting in equations (3)–(4) and using equation (9), q is found to be $\pi/2$. The compatibility of (3) and (4) for non-vanishing perturbation amplitudes leads to an expression for $H_\perp$ as a function of the wave vector:

$$\omega_H(Q_x) = \frac{\delta_1 Q_x^4 + \delta_2 Q_x^2 + \delta_3}{\beta_1 Q_x^2 + \frac{\pi^2}{4}}; \quad Q_x = q_x h;$$

$$\omega_H = \frac{\chi_A H_\perp^2 h^2}{K_1}; \quad \beta_1 = \frac{\varepsilon_\parallel}{\varepsilon_\perp}; \quad \beta_3 = \frac{K_3}{K_1}; \quad \delta_1 = \beta_1 \beta_3;$$

$$\delta_2 = \omega_E + \frac{\pi^2}{4}(\beta_1 + \beta_3); \quad \delta_3 = \frac{\pi^2}{4}\left(\omega_E + \frac{\pi^2}{4}\right). \quad (12)$$

Clearly, when $Q_x \to 0$, $H_\perp(Q_x)$ reduces to H_F (11). Also, $H_\perp(Q_x)$ depends on Q_x^2 showing that the sign of Q_x is unimportant. Suppose E_{xo} is high enough. Due to the net destabilizing action of $\mathbf{E}'$, $H_\perp(Q_x)$ diminishes when Q_x is increased from zero, reaching a minimum $H_{PX} = H_\perp(Q_{PX})$ when $Q_x = Q_{PX}$. Further increase of q_x causes an increase in $H_\perp(Q_x)$; hence, H_{PX} and Q_{PX} can be regarded as the X magnetic threshold and (dimensionless) wave vector at threshold, respectively. From equation (12),

$$Q_{PX}^2 = \frac{\pi^2}{4\beta_1}(\Delta - 1); \quad \Delta^2 = 1 + \frac{16\beta_1}{\delta_1 \pi^4}\left(\beta_1 \delta_3 - \frac{\delta_2 \pi^2}{4}\right);$$

$$H_{PX}^2 = \left(2\delta_1 Q_{PX}^2 + \frac{\delta_2}{\beta_1}\right)\frac{K_1}{\chi_A h^2}. \quad (13)$$

It is convenient to define a reduced X threshold in terms of H_F from equation (11):

$$r_X = \frac{H_{PX}}{H_F}.$$

When $r_X < 1$, the X Mode is more favourable than HD. Clearly, as E_{xo} increases, Q_{PX} increases and r_X diminishes. When E_{xo} is sufficiently low, Q_{PX} vanishes. In this limit, the X and HD thresholds become equal leading to the critical electric field E_1,

$$E_1^2 = \frac{\pi^3 K_3 \varepsilon_\perp^2}{h^2 \varepsilon_\parallel \varepsilon_A^2}. \quad (14)$$

For $E_{xo} < E_1$, the X Mode cannot exist and only HD is possible. It is instructive to compare E_1 with E_M (see equation (18) of [21]). E_M can be obtained from E_1 by substituting K_1 for K_3 and interchanging the dielectric constants. The reduced electric field R_E is defined using E_1,

$$R_E = \frac{E_{xo}}{E_1}.$$

The X Mode occurs only when $R_E > 1$. Increase of E_1 implies an increased width of the region of existence of HD.

While HD involves only a splay deformation, X Mode is associated with both splay and bend. This actually increases the elastic free energy of X Mode relative to that of HD [note the term $K_3 \theta_{,x}^2$ in equation (2)] causing an additional stabilizing torque $K_3 \theta_{,xx}$ in equation (4). However, $\mathbf{E}$ for the X Mode contains two perturbations, $E_x' = -\psi_{,x}$ and $E_z' = -\psi_{,z}$ both of which vary periodically with x. Of these, E_z' (destabilizing component) is in phase with θ along x while E_x' (stabilizing component) is out of phase. In addition, E_z' is symmetric (like θ) while E_x' is antisymmetric. Hence, the destabilizing effect of E_z' is felt more strongly than the stabilizing influence of E_X'. Once the additional stabilizing influence of bend is overcome [note K_3 in the numerator of equation (14)], the X Mode sets in; as the torque due to $\mathbf{E}'$ is $\varepsilon_A E_{xo} \psi_{,z}$ in equation (4), this happens when E_{xo} is sufficiently strong. The higher the ε_A, the stronger is this torque due to $\mathbf{E}'$. Hence, ε_A appears in the denominator of equation (14). To understand this more formally, E_1 is differentiated with respect to one of the variables, keeping the others fixed. Then, $\partial E_1/\partial \varepsilon_a$, $\partial E_1/\partial \varepsilon_\parallel < 0$ and $\partial E_1/\partial K_3$, $\partial E_1/\partial \varepsilon_\perp > 0$ all of which supports the above qualitative arguments.

With the parameters (10), r_X and Q_{PX} are studied as functions of R_E [curves 2 in figures 1(*a*) and 1(*b*)] with a sample thickness $2h = 500\,\mu m$. The study of reduced quantities makes the results independent of sample thickness. When R_E assumes high values, r_X tends asymptotically to a lower limit. From equations (11)–(13), $r_X \approx (\varepsilon_\perp/\varepsilon_\parallel)^{1/2}$ when $R_E \gg 1$; in the same limit, $Q_{PX} \approx (\pi^2 R_E/4\beta_1)^{1/2}$. Interestingly, this limit is independent of the elastic constants. For sufficiently low R_E, the wavelength of periodicity $\sim 2h$. Relevant quantities for SOLUTION 2 can be calculated by substituting 2π for π in equations (11) and (12). Results are not presented for SOLUTION 2 as it has higher threshold than SOLUTION 1 and is, therefore, of no interest. This is because an antisymmetric θ is the *next higher harmonic* to the symmetric θ and hence the elastic deformation energy of SOLUTION 2 is higher than that of SOLUTION 1.

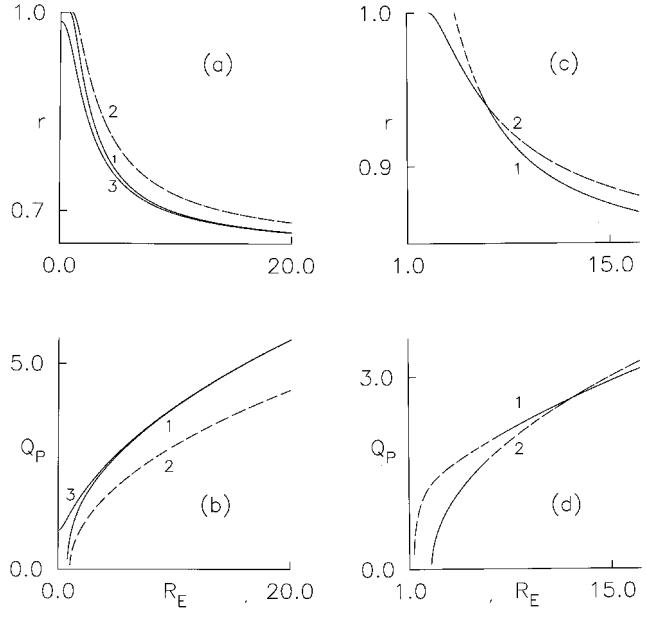

Figure 1. Plots of r_X, r_Y, Q_{PX}, Q_{PY} as functions of R_E under rigid anchoring hypothesis (see § 3.1 and § 3.2 for definitions). The material chosen is 5CB with parameters (10). The planar orientation is stabilized by $\mathbf{E}_0$ along x and destabilized by $\mathbf{H}_\perp$ applied in the yz plane making angle α radian with y axis. r_X and r_Y are the reduced magnetic thresholds for the X and Y Modes, respectively. Q_{PX} and Q_{PY} are the reduced wave vector amplitudes for the two Modes. Curves 1 and 2 represent, respectively, the Y and the X Modes; a dashed curve denotes a region of no real interest. Diagrams are drawn for $\alpha = (a, b)\pi/2, (c, d)$ 0·8 rad. In (a, b), both Modes conform to the symmetries of SOLUTION 1. In (c, d), the X Mode possesses the symmetry of SOLUTION A and exhibits a critical point with HD; the Y Mode is a mixture of SOLUTIONs 1 and 2 and hence does not possess a critical point in the low R_E region. The crossover from Y Mode to X Mode is evident in (c, d). Curve 1 in (c) has not been exhibited fully where $r_Y > 1$. Curves 3 in (a, b) represent the Y Mode for a hypothetical material with $K_1 = 4K_2$. The critical point between HD and Y Mode disappears in this case as the Y Mode exists even when $E_{xo} = 0$ (see also § 5.2).

Calculations for the Y Mode proceed similarly except that now all three variables enter the picture. While θ and ψ are in phase along y [say, with a variation of $\sin(q_y y)$], ϕ is out of phase [with the dependence $\cos(q_y y)$]. The two uncoupled solutions are referred to as before as θ and ψ have the same symmetry as the X Mode:

Y Mode SOLUTION 1: θ is symmetric; ψ and ϕ are antisymmetric.

Y Mode SOLUTION 2: θ is antisymmetric; ψ and ϕ are symmetric.

Even though the Y Mode has periodicity along y (normal to the initial alignment), the perturbations conform to definite spatial symmetries because $\mathbf{H}_\perp$ acts along z which is a symmetry direction.

Clearly, SOLUTION 1 involves lower deformation energy than SOLUTION 2. The net destabilization influence due to $\mathbf{E}'$ is also stronger for SOLUTION 1. Once y dependence is separated out of equations (3)–(5), three coupled ordinary differential equations result, each of second order. These are solved by the series solution method with boundary conditions (9) to yield a compatibility condition from which one obtains the neutral stability curve $H_\perp(Q_y)$ where $Q_y = q_y h$. The minimum $H_{PY} = H_\perp(Q_{PY})$ occurring at $Q_y = Q_{PY}$ is taken as the Y threshold; the reduced magnetic Y threshold is defined in terms of H_F of equation (11) as $r_Y = H_{PY}/H_F$. Computation for equation (10) shows that $r_Y < r_X$ for all R_E [figures 1 (a) and 1 (b); curves 1] with the critical point for Y Mode also lying below that of X Mode ($R_E = 1$). The reason for this is obvious from equations (3)–(5). In comparison with HD, the additional elastic deformation in the X Mode is the bend while the corresponding distortion in the Y Mode is the twist [$K_2\theta_{,yy}$ in equation (4)]. The decrease in free energy caused by this is partially offset by the antisymmetricity of ϕ which introduces additional splay and twist contributions [$K_1\phi_{,yy}$ and $K_2\phi_{,zz}$ in equation (5)]. The X Mode has only one destabilizing contribution from $\psi_{,z}$ in equation (4); the Y Mode benefits from this and also from the additional destabilizing torque $\sim\psi_{,y}$ in equation (5). This may account for the Y Mode being more favourable than the X Mode. The Y Mode is associated with antisymmetric ϕ, but ϕ does not appear in HD. No direct coupling exists between ϕ and $\mathbf{H}_\perp$ in the present case. The existence of the critical point between the Y Mode and HD is an indication that the amplitude of ϕ depends on Q_{PY} so that ϕ disappears when $Q_{PY} \to 0$.

In a nematic with $K_1 > 3{\cdot}4K_2$, the Y Mode results instead of HD when $\mathbf{H}_\perp$ acts along z even in the absence of $\mathbf{E}_o$ [6, 8] (see also § 5). For parameters (10), however, the Y Mode cannot set in unless E_o is impressed; only HD exists. The Y Mode develops in 5CB (10) when the lack of elastic anisotropy is compensated by the destabilizing contribution arising from $\mathbf{E}'$ [figures 1 (a) and 1 (b)]. A critical point ($\approx 0{\cdot}8R_E$) exists between the Y Mode and HD owing mainly to the deficiency in elastic anisotropy of equation (10). It is, therefore, possible that a material with parameters (10) but a high enough elastic anisotropy will not have a critical point; in such a case, the Y Mode would develop for any R_E and HD would never set in. This conjecture proves true for a hypothetical material with parameters (10) except that $K_1 = 4K_2$ [curves 3 in figures 1 (a) and 1 (b)]. With increase of R_E, the stripe width and r_Y decrease due to the enhanced destabilizing torque resulting from $\mathbf{E}'$ [see terms $\sim E_{xo}\psi_{,z}$ and $E_{xo}\psi_{,y}$ in equations (4) and (5)].

Presently, we shall contrast this behaviour with that exhibited by a similar material in a different geometry (§ 5.2).

The XY Mode can also be studied. The x, y variation is $\sin Q/h(C_\mu x + S_\mu y)$ for θ and ψ and $\cos Q/h(C_\mu x + S_\mu y)$ for ϕ; μ is the angle between the dimensionless wave vector of magnitude Q and the x axis. With this *ansatz*, equations (3)–(5) reduce to a set of ordinary differential equations which support the same modal structure as for the Y Mode. The solution effected with the series method yields a neutral stability surface $H_\perp(Q, \mu)$. For $\mu = 0$, the neutral stability surface degenerates into the neutral stability curve for the X Mode whose minimum yields the X threshold. Similarly, the Y threshold results at $\mu = \pi/2$. Calculation shows that when R_E is sufficiently high, the absolute minimum of the neutral stability surface lies at $\mu = \pi/2$, corresponding to the Y threshold; no other minimum can be found at other μ values. Thus, the XY Mode degenerates into the Y Mode. This is to be expected because the free energy density for the XY Mode results from that of the Y Mode by the addition of two purely positive terms, $K_3\theta_{,x}^2$ and $K_3\phi_{,x}^2$. These correspond to purely stabilizing elastic torques, $K_3\theta_{,xx}$ and $K_3\phi_{,xx}$. Naturally, no point on the neutral stability surface can dip below the Y threshold. Hence, the XY Mode is not studied.

3.2. *Results for rigid anchoring with $\alpha \neq \pi/2$*

Now $\mathbf{H}_\perp$ is tilted away from z in the yz plane at different α. With dependence on z (HD), all three perturbations are coupled. Equations (3)–(5) yield a pair of coupled ordinary differential equations in θ and ϕ. For symmetric θ and ϕ, the z dependence $\sim\cos(\pi z/2h)$ leads to the HD threshold,

$$H_F^2(\alpha) = \frac{(K_1\varepsilon_\perp\pi^3 + \varepsilon_A\varepsilon_\parallel h^2E_{xo}^2)(K_2\pi^3 + \varepsilon_A h^2E_{xo}^2)}{4\pi\chi_A h^2[\varepsilon_\perp\pi^3(K_1C_\alpha^2 + K_2S_\alpha^2) + \varepsilon_A h^2E_{xo}^2(\varepsilon_\parallel C_\alpha^2 + \varepsilon_\perp S_\alpha^2)]} \tag{15}$$

which is a function of α. When $\alpha = \pi/2$, equation (15) reduces to (11) with ϕ decoupling from θ and ψ. If $\mathbf{H}_\perp$ acts along y, θ and ψ damp out and (15) yields

$$\frac{\chi_A h^2H_F^2(\alpha = 0)}{K_2} = \frac{\pi^2}{4} + \Omega_E; \quad \Omega_E = \frac{\varepsilon_A h^2E_{xo}^2}{4\pi K_2} \tag{16}$$

which is obtained from (5) alone. The absence of the ratio $\varepsilon_\parallel/\varepsilon_\perp$ shows the non-existence of electric modulations for a twist HD, leading to the following conclusion. As the tilt of $\mathbf{H}_\perp$ is varied away from z towards y, the coupling between ψ and the director deformations diminishes. As both PD Modes at $\alpha = \pi/2$ arise from the destabilizing influence of ψ, the X and Y thresholds should increase relative to the HD threshold when α is diminished from $\pi/2$. At sufficiently low α, both PD Modes should be quenched. If the rate of increase of threshold for α variation is different for the X and Y Modes, a crossover might even occur from the Y to the X Mode.

For the X Mode, equations (3)–(5) support two decoupled solutions:

X Mode SOLUTION A: θ and ϕ are even; ψ is odd.
X Mode SOLUTION B: θ and ϕ are odd; ψ is even.

The X Mode perturbations exhibit definite spatial symmetry as the direction of periodicity (x) is along the optic axis and $\mathbf{H}_\perp$ acts in a plane normal to x. Compared with the case $\alpha = \pi/2$, the X Mode is associated with the additional perturbation ϕ whose presence only adds to the elastic free energy without introducing additional destabilizing torques via modification of $\mathbf{E}$. Thus, ϕ only adds stabilizing torques whose magnitude increases as α is diminished from $\pi/2$. Hence, the X Mode gets suppressed in favour of HD when $\mathbf{H}_\perp$ is rotated away from z.

Clearly, SOLUTION A has the same symmetry as HD and can be regarded as an extension of HD. As all three perturbations are in phase along x, the *ansatz*

$$(\theta, \phi, \psi) = \left[\theta_M\cos\left(\frac{\pi z}{2h}\right), \phi_M\cos\left(\frac{\pi z}{2h}\right), \psi_M\sin\left(\frac{\pi z}{2h}\right)\right] \times \sin\frac{Q_x x}{h}$$

satisfies equation (9) as well as symmetry requirements. Substitution in equations (3)–(5) leads to a compatibility condition and the neutral stability curve, $H_\perp(Q_x)$:

$$\frac{\chi_A h^2H_\perp^2}{K_1} = \frac{\gamma_1Q_x^6 + \gamma_2Q_x^4 + \gamma_3Q_x^2 + \gamma_4}{\gamma_5Q_x^4 + \gamma_6Q_x^2 + \gamma_7};$$

$$\beta_2 = \frac{K_3}{K_2}; \quad \gamma_1 = \beta_1\beta_2\beta_3;$$

$$\gamma_2 = \frac{\pi^2}{4}[\beta_3\beta_2 + \beta_1(\beta_2 + \beta_3)] + 2\beta_2\omega_E;$$

$$\gamma_3 = \frac{\pi^4}{16}(\beta_1 + \beta_2 + \beta_3) + \Omega_E\omega_E + \frac{\pi^2}{4}[\omega_E + \Omega_E(\beta_1 + \beta_3 + \beta_1\beta_3)];$$

$$\gamma_4 = \frac{\pi^2}{4}\left(\frac{\pi^2}{4} + \omega_E\right)\left(\frac{\pi^2}{4} + \Omega_E\right); \quad \gamma_5 = \beta_1\beta_2;$$

$$\gamma_6 = \Omega_E\beta_1 + \frac{\pi^2}{4}\left[\beta_2 + \beta_1\left(C_\alpha^2\frac{\beta_2}{\beta_3} + S_\alpha^2\right)\right];$$

$$\gamma_7 = \frac{\pi^2}{4}\left[\frac{\pi^2}{4}\left(C_\alpha^2\frac{\beta_2}{\beta_3} + S_\alpha^2\right) + \Omega_E(S_\alpha^2 + C_\alpha^2\beta_1)\right]. \tag{17}$$

At a given α and sufficiently high R_E, the X threshold H_{PX} is the minimum of (17) occurring at $Q_x = Q_{PX}$. The reduced threshold $r_X = H_{PX}/H_F$ is defined using H_F of (15). As the X Mode is an extension of HD, a critical point can be expected between the X Mode and HD where $Q_{PX} \to 0$.

The case of Y Mode is not so simple. When $\mathbf{H}_\perp$ acts at some arbitrary α in the yz plane, its direction is not symmetric relative to the direction of periodicity (y). As seen from equations (4) and (5), magnetic cross coupling terms involving $\chi_A H_\perp^2 S\alpha C\alpha$ arise connecting ϕ and ϕ_{zz} as well as θ and θ_{zz}. A closed form solution cannot be obtained with each perturbation possessing a unique spatial symmetry as in SOLUTION 1 or SOLUTION 2. Each perturbation becomes the sum of two terms as in

$$\theta = \theta_U \cos\frac{Q_y y}{h} + \theta_T \sin\frac{Q_y y}{h}$$

where θ_U, θ_T, etc. are functions of z. Substitution in equations (3)–(5) yields six coupled ordinary differential equations in θ_U, ϕ_T, etc. From (9), six boundary conditions also result. If θ_T, ϕ_T and ψ_U are even, then θ_U, ϕ_U and ψ_T are odd. Thus, each perturbation is a linear superposition of two terms of which one conforms to the symmetry of SOLUTION 1 and the other to the symmetry of SOLUTION 2. The presence of SOLUTION 2 elevates the elastic deformation energy and diminishes the destabilizing contribution from $\mathbf{E}'$. The proportion of SOLUTION 2 increases as α is diminished from $\pi/2$. Hence, the Y Mode becomes unfavourable at sufficiently low α.

At suitable α and R_E, the series solution method is applied to equations (3)–(6) and (9) and the Y threshold numerically calculated as the minimum $H_{PY} = H_\perp(Q_{PY})$ of the neutral stability curve $H_\perp(Q_y)$. The reduced magnetic threshold $r_Y = H_{PY}/H_F$ is defined using H_F of (15). As the Y Mode perturbations have no unique spatial symmetry at general α, the Y Mode and HD are not separated by a critical point where Q_{PY} vanishes. In general, Q_{PY} is non-zero when r_Y attains unity so that the transition from Y Mode to HD occurring at low R_E is one of the first order, assuming Q_{PY} to be the order parameter.

The results for both Modes reduce to those of figures 1 (a) and 1 (b) (curves 1 and 2) when α is close to $\pi/2$; the Y Mode is more favourable than the X Mode over the entire R_E range except that HD prevails when R_E is very small. This is to be expected as the proportion of SOLUTION 2 is minimal when α is close to $\pi/2$ so that the perturbations have almost the spatial symmetry of SOLUTION 1. The discontinuity of the transition between the Y Mode and HD is also imperceptible. When α is higher ($\mathbf{H}_\perp$ rotated away from the z axis), marked deviations occur in the variation of threshold parameters. The R_E variation at $\alpha = 0{\cdot}8$ rad bears this out [figures 1 (c) and 1 (d)]. The Y Mode is more favourable that the X Mode at high R_E. When R_E is diminished, a crossover occurs between the two Modes with the X Mode becoming more favourable than the Y Mode. This should be accompanied by a discontinuous change in the wave vector of periodicity (change in direction by $\pi/2$ rad and a decrease in the stripe width). At this α, the X Mode critical point is higher than $R_E = 1$. In this region, the Y Mode is of academic interest as the Y threshold cannot meet the HD threshold continuously and $r_Y > 1$.

The variation of α at fixed R_E (figure 2) complements the conclusions of figure 1. The Y Mode is more favourable than the X Mode when α is close to $\pi/2$. When α is decreased, a crossover occurs from the Y to the X Mode accompanied by discontinuous change in the wave vector. In this region again, $r_Y > 1$. When α is low enough, even the X Mode disappears below a critical point and HD alone exists. When R_E is diminished, the α ranges of existence of both PD Modes shrink [figures 2 (c) and 2 (d)]. Then, HD appears over a wider α range starting from $\alpha = 0$. The Y threshold exceeds the X threshold with decrease of α because of the larger

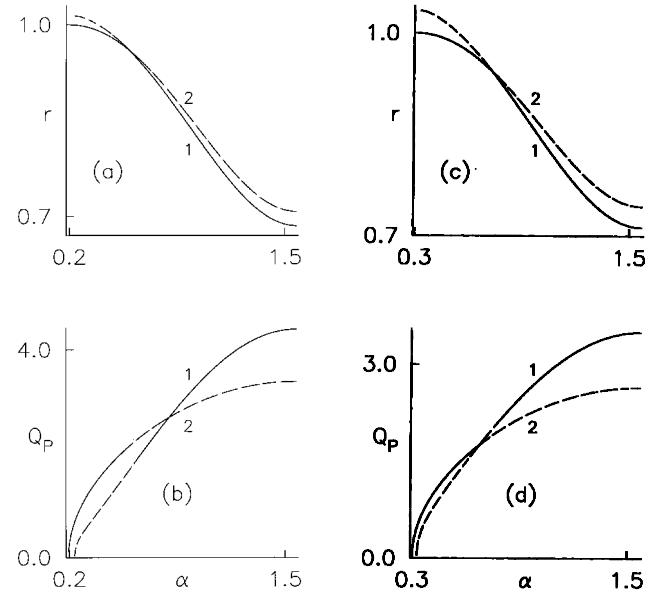

Figure 2. Variation of r_X, r_Y, Q_{PX}, Q_{PY} with α for 5CB parameters (10) at $R_E = (a, b)$ 12·5, (c, d) 8 (see § 3.2 and figure 1 for details). The X Mode (curve 2) conforms to SOLUTION A (and exhibits a critical point with HD); and Y Mode (curve 1) does not exhibit a critical point as it is a mixture of SOLUTIONs 1 and 2 (§ 3.1). The crossover from Y Mode to X Mode occurs when $\mathbf{H}_\perp$ is rotated from z towards y. The α range of existence of both PD Modes shrink when R_E is decreased.

proportion of the unfavourable SOLUTION 2 getting mixed with SOLUTION 1.

The XY Mode solution is analogous to that of the Y Mode. The XY Mode perturbations also do not possess pure spatial symmetry. Closed form solutions are in the form

$$\phi = \phi_U \cos\left[\frac{Q(C_\mu x + S_\mu y)}{h}\right] + \phi_T \sin\left[\frac{Q(C_\mu x + S_\mu y)}{h}\right]$$

where ϕ_U, θ_T, ψ_T belong to SOLUTION 1 and ϕ_T, θ_U, ψ_U belong to SOLUTION 2. The compatibility condition obtained from equations (3)–(5) and (9) using the series solution method enables definition of the neutral stability surface $H_\perp(Q, \mu)$ at given R_E and α. $H_\perp(Q, \mu)$ does not exhibit an absolute minimum at arbitrary μ. When R_E and α are sufficiently high the XY threshold occurs at $\mu \approx \pi/2$ corresponding to the Y threshold itself. At low α, the XY threshold degenerates into the X threshold occurring at $\mu \approx 0$. Hence, the XY Mode is not studied.

Figures 1 and 2 indicate the shape of the phase boundaries between the different deformations in the R_E–α plane. For the Y Mode, the phase boundary is obtained by initially fixing R_E at a high value. Starting with α close to $\pi/2$, r_Y and Q_{PY} are determined. Now α is diminished in small steps and the above calculation performed for each α. At some $\alpha = \alpha_Y$, $r_Y = 1$. If α is decreased further, r_Y exceeds unity. Generally, Q_{PY} is non-zero at this point. The value of R_E is decremented and the above procedure repeated. A plot of R_E versus α_Y yields the phase boundary separating the Y Mode and HD. A similar calculation yields the phase boundary for the X Mode except that when $\alpha \to \alpha_X$, $Q_{PX} \to 0$.

Figure 3 (*a*) contains the phase boundaries of the X and Y Modes for 5CB parameters and is in qualitative agreement with the conclusions of figures 1 and 2. The following points are apparent.

(i) HD sets in at low α (when $\mathbf{H}_\perp$ is rotated close to the y axis) as well as at low R_E; this region is marked HD.

(ii) In the region marked X, only the X Mode exists with threshold lower than that of HD.

(iii) The region marked with X and Y is one where both X and Y Modes can exist as solutions with thresholds lower than the HD threshold. Here, an explicit calculation of r_Y and r_X will reveal which of the two Modes has the lower threshold and is, therefore, the more favourable one.

(iv) The Y Mode alone prevails in a small triangular region near $\alpha = \pi/2$.

Figure 3 (*b*) shows the phase diagrams for a hypothetical material having parameters (10) but with $K_1 = 4K_2$. This diagram is similar to figure 3 (*a*) except that the Y Mode occurs even at $E_{xo} = 0$ when $\mathbf{H}_\perp$ acts close to the z axis. Clearly this is by virtue of the elastic anisotropy of the material (the Y region near the right-side bottom is now enlarged and extends right down to $R_E = 0$).

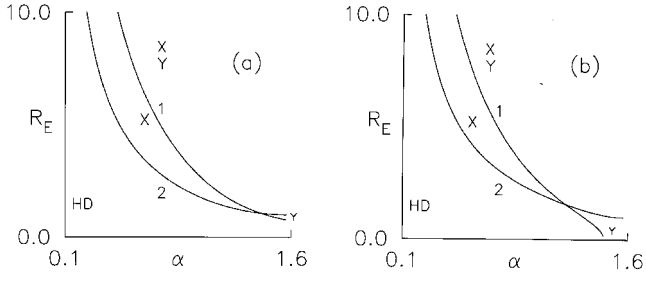

Figure 3. (*a*) Phase boundaries of the X (curve 2) and Y (curve 1) Modes in the R_E–α plane for 5CB parameters (10) with rigid anchoring. The X Mode is SOLUTION A while the Y Mode is a superposition of SOLUTIONs 1 and 2 for general α. (*b*) Phase boundaries for a hypothetical material with $K_1 = 4K_2$. The Y Mode exists even in the absence of $\mathbf{E}_o$ due to the high elastic anisotropy (see § 3.2 and figure 1 for details).

4. Material with positive ε_A and χ_A; weak anchoring

The boundary conditions (7)–(8) are now employed. In general, both θ and ϕ may occur; hence, both anchoring strengths may affect the onset of distortion. For simplicity, we assume, in § 2, that the polar (or azimuthal) anchoring strength at either boundary is equal. As the anchoring energy is finite, the bulk elastic torque induces a deformation at the boundaries which, in turn, affects the nature of restrictions placed on ψ, as $\psi_{,z}$ will also not vanish at the boundaries. It is also not straightforward to scale results to make them independent of the sample thickness; hence, the sample thickness becomes a parameter in the problem. The boundary conditions for different deformations are different; even in the most general case, K_{24} will not affect either HD or the X Mode. Boundary conditions for the Y and XY Modes, on the other hand, contain K_{24}. As the wavelength of periodicity $\sim 2h$, the influence of K_{24} becomes important if $Bh \sim K_{24}$. As $K_{24} \sim 10^{-7}$ dyne, $h \sim 10^{-5}$ cm for K_{24} to be effective if the relevant anchoring strength $B \sim 10^{-2}$ erg cm^{-2}. Such a sample thickness is available in the sub-micron cavities in PDLC films. In thicker samples, the effect of K_{24} is less significant. If, on the other hand, the anchoring is still weaker, effects of K_{24} may be seen even in thick samples.

4.1. *Results for weak anchoring with $\alpha = \pi/2$*

With $\mathbf{H}_\perp$ acting along z, the results are especially simple in some cases. For HD, ϕ damps out leaving θ

coupled to ψ; only B_θ is now relevant. From equations (3), (4) and (7), the HD threshold is found:

$$H_F^2 = \frac{K_1}{\chi_A h^2}(q_C^2 + \omega_E);$$

$$\sigma_\theta \cos q_C - q_C \sin q_C = 0; \quad \sigma_\theta = \frac{B_\theta h}{K_1}. \tag{18}$$

For a given B_θ and other parameters, q_C is numerically determined by iteration; then H_F is computed. When $\sigma_\theta \gg 1$, $q_C \approx \pi/2$ and (18) reduces to (11). In general, q_C (or equivalently H_F) diminishes when σ_θ is decreased.

The structure of the X Mode remains the same as that for rigid anchoring. Again, ϕ does not appear; θ and ψ are in phase along x and possess the symmetries of SOLUTION 1 or SOLUTION 2. Proceeding as in § 3.1, the neutral stability curve for the X Mode is determined from

$$\sigma_\theta(q_1^2 + q_2^2)\cos q_1 - q_1(\beta_1 Q_x^2 + q_1^2)\sin q_1 + q_2(q_2^2 - \beta_1 Q_x^2)(\cos q_1)\tanh q_2 = 0;$$

$$q_1^2 = \frac{(P_1^2 + 4P_2)^{1/2} + P_1}{2}; \quad q_2^2 = \frac{(P_1^2 + 4P_2)^{1/2} - P_1}{2};$$

$$P_1 = \omega_H - \omega_E - Q_x^2(\beta_1 + \beta_3);$$

$$P_2 = Q_x^2[\beta_1(\omega_H - \beta_3 Q_x^2) - \omega_E]. \tag{19}$$

The X threshold is affected only by B_θ, the polar anchoring strength, and is independent of B_ϕ, the azimuthal anchoring strength. For strong polar anchoring, ($\sigma_\theta \gg 1$), equation (19) reduces to $\cos q_1 \approx 0$ or $q_1 \approx \pi/2$ leading to equation (12) for rigid anchoring. Hence, results of X Mode from (19) should reduce to those of (12) when the anchoring is strong. The reduced X threshold is calculated in terms of H_F (18). The X Mode and HD need to be compared. The perturbations of both deformations possess identical spatial symmetry for z dependence; they also obey identical boundary conditions. But for the X Mode condition (8) has to be separately imposed while for HD it is identically satisfied once (3) is integrated. Because of this reason even if a field, say $E_{xo} = E_A$, exists where $Q_{PX} \to 0$, r_X may exceed unity in this limit. Thus, E_A cannot be a true critical point separating HD and the X Mode. When equation (19) is expanded in powers of Q_x and (18) used, (19) takes the form $N_1 Q_x^2 = 0$ to lowest order in Q_x where N_1 is a function of material parameters, anchoring strength and E_{xo}. Equating N_1 to zero and solving for E_{xo}, one gets

$$E_A^2 = \frac{q_C^2}{q_C^2 + \sigma_\theta^2}\left(\frac{\beta_3}{\beta_1}(\sigma_\theta^2 + \sigma_\theta + q_C^2) - \sigma_\theta\right)\frac{4\pi K_1 \varepsilon_\perp}{\varepsilon_A^2 h^2}. \tag{20}$$

When $\sigma_\theta \gg 1$, $E_A \approx E_1$ of (14). When σ_θ is diminished (the polar anchoring is weakened), q_C has to be first computed and E_A calculated subsequently. For uniformity, R_E is calculated as before in terms of E_1, equation (14).

For the Y Mode, the equations for equilibrium in the bulk (3)–(5) are the same as those for rigid anchoring, but the boundary conditions (7) and (8) are different. Out of the two uncoupled solutions, SOLUTION 1 is selected. The Y threshold is determined numerically using the series solution method and depends on K_{24}, σ_θ and

$$\sigma_\phi = \frac{B_\phi h}{K_2}.$$

The dimensionless Y threshold, r_Y, is also calculated in terms of H_F (18). The difference in the boundary conditions of HD and the Y Mode arises from the terms $\sim(K_1 - K_{24})\phi_{,y}$ and $\sim(K_{24} - K_2)\theta_{,y}$ in (7). This difference should disappear in the limit of vanishing wave vector q_y. The other difference is the appearance of ϕ in the Y Mode but not in HD. If the amplitude of the Y Mode ϕ is proportional to some power of q_y, then ϕ will vanish with the wave vector; in other words, a critical point will exist between HD and the Y Mode.

The variations of r_X and r_Y with R_E are similar to those of figures 1 (*a*) and 1 (*b*) (curves 1 and 2) for a thick sample ($h = 250\,\mu m$) and strong anchoring ($B_\theta, B_\phi \sim 10^{-2}$ dyne cm^{-1}). The Y Mode is uniformly more favourable than the X Mode, hence the X threshold is not depicted. Weakening of anchoring strength by four orders of magnitude or changing the value of K_{24} from zero to $2K_2$ has little effect on the results. The effect of weak anchoring becomes apparent only in a thin sample with $h = 2{\cdot}5\,\mu m$. A detailed calculation involves not only choosing different sets of values for the two anchoring strengths but also for K_{24}. To reduce the bulk of presentation, the Y threshold parameters are plotted (figure 4) against R_E for three extreme sets of anchoring strengths:

- (*a*, *b*) strong polar anchoring, weak azimuthal anchoring;
- (*c*, *d*) weak polar anchoring, strong azimuthal anchoring;
- (*e*, *f*) weak polar and azimuthal anchoring.

Two extreme values are chosen for K_{24}—zero and $2K_2$. The case of strong polar and azimuthal anchoring is left out as the results are similar to those of figures 1 (*a*) and 1 (*b*) (curve 1) and the influence of K_{24} is hardly significant. Regardless of the anchoring strengths, enhancement of K_{24} has a salutory effect on the formation of the Y Mode; in general, the Y threshold decreases at a given R_E, the stripes become narrower (wave vector increases) and the R_E range of existence of the Y Mode widens with respect to that of HD. This is clearly because of

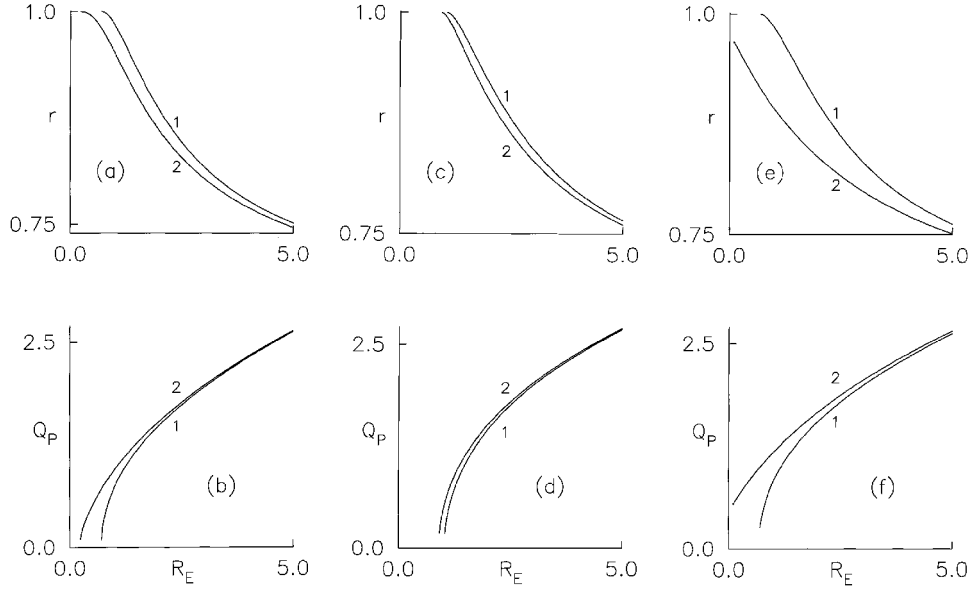

Figure 4. Plots of r_Y versus R_E when director anchoring energy is finite and the sample thin ($h = 2{\cdot}5\,\mu m$). $\mathbf{H}_\perp$ acts along z so that the Y Mode perturbations conform to definite spatial symmetry. r_X (the reduced magnetic threshold of the X Mode) is omitted as it is higher than r_Y for all R_E. Parameters used are from (10) for 5CB with $(B_\theta, B_\phi) = (a, b)$ $(10^{-2}, 10^{-6})$, (c, d) $(10^{-6}, 10^{-2})$, (e, f) $(10^{-6}, 10^{-6})\,erg\,cm^{-2}$. The curves are drawn for $K_{24} = (1)$ zero (2) $2K_2$ (see § 4.1).

the opposing role of the K_{24} surface torque (7) with respect to those corresponding to K_1 and K_2. Obviously, the effect of K_{24} is most pronounced when both anchoring strengths are weak [figures 4 (*e*) and 4 (*f*)] with the Y Mode appearing to form even in the absence of R_E; this result is in qualitative agreement with the findings of [28]. A diminution of B_ϕ widens the range of existence of the Y Mode—compare figures 4 (*a*) and 4 (*b*) with 4 (*c*) and 4 (*d*). A reason for this is that development of the twist, ϕ, is central to the formation of the Y Mode. Decrease of B_ϕ makes it easier for ϕ to form through the action of electric perturbations—for 5CB (10), the elastic anisotropy is not high enough to induce Y Mode in the absence of **E**.

4.2. *Results for weak anchoring with* $\alpha \neq \pi/2$

As in § 3.2, the governing equations for the X Mode support two uncoupled solutions of which we choose SOLUTION A. The Y Mode is a mixture of SOLUTIONs 1 and 2 superposed out of phase along y. The full set of boundary conditions (7)–(8) is employed. As the X Mode now involves ϕ, its threshold is influenced by both anchoring strengths (unlike the situation in § 4.1). The thresholds are computed by the series solution method. When both anchorings are strong (say, $B_\theta, B_\phi \sim 10^{-2}\,erg\,cm^{-2}$), the results become almost identical to those of figures 1 (*c*), 1 (*d*) and 2. At a given R_E, the Y Mode is more favourable when α is close to $\pi/2$; the X threshold dips below that of the Y Mode when $\mathbf{H}_\perp$ is rotated sufficiently away from z. At a given α (sufficiently removed from $\pi/2$), the Y Mode is more favourable than the X Mode at high R_E while the reverse holds when R_E is decreased to low values.

A detailed exposition of the effects of anchoring strengths is cumbersome. The influence of the anchoring strengths on the ranges of existence of the X and Y Modes can be appreciated by choosing the three extreme cases of § 4.1 even for a thick sample (figure 5) when $\mathbf{H}_\perp$ acts roughly midway between the z and y axes. The nature of variation of threshold parameters is similar to that found in figures 1 (*c*) and 1 (*d*) with the Y Mode becoming unfavourable when $R_E < 6$. K_{24} has been equated to zero because its effect on the Y Mode is felt only at low R_E where the Y Mode is of only academic interest. The range of existence of the Y Mode widens when B_ϕ is diminished [compare figures 5 (*c*) and 5 (*d*) with 5 (*a*) and 5 (*b*)]; diminution of B_θ does not have much effect [compare figures 5 (*c*) and 5 (*d*) with 5 (*e*) and 5 (*f*)]. The Y Mode exhibits a strong discontinuity of threshold with HD in the low R_E region with the wave vector remaining non-zero when $r_Y = 1$.

As the X Mode survives in the low R_E region, one can compare the diagrams to find out how changes in anchoring strengths affect this Mode. In general, $Q_{PX} \to 0$ when $r_X \to 1$. The range of existence of the X Mode widens when the polar anchoring is weakened [figures 5 (*a–d*)]. Weakening of the polar anchoring makes it easier for the θ deformation to set in. As θ is the principal deformation of the X mode which causes destabilizing electric perturbations, a factor aiding the formation of θ

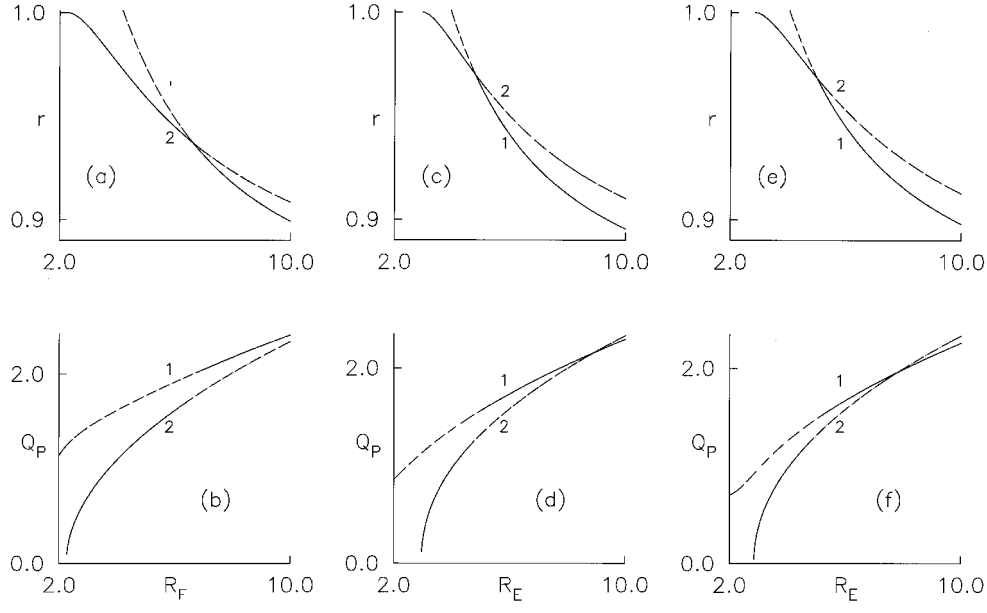

Figure 5. Variations of r_X, r_Y, Q_{PX} and Q_{PY} versus R_E for weak anchoring; parameters as in expression (10) and $h = 250\,\mu m$. $\mathbf{H}_\perp$ acts in the yz plane making angle $\alpha = 0{\cdot}8$ rad with the z axis (see figure 1 for details). Curves 1 and 2 represent, respectively, the Y and X Modes. Curve 1 has not been fully shown in the low R_E limit in (a, c, e) where r_Y exceeds unity. Diagrams are drawn for $(B_\theta, B_\phi) = (a, b)\ (10^{-6}, 10^{-2})$, $(c, d)\ (10^{-2}, 10^{-6})$, $(e, f)\ (10^{-6}, 10^{-6})\,erg\,cm^{-2}$. K_{24} is assumed to be zero (see § 4.2).

should widen the range of existence of the X Mode. From figures 5 (*a*), 5 (*b*), 5 (*e*) and 5 (*f*) the critical point of the X Mode is found to move to slightly higher R_E when the azimuthal anchoring is weakened. In the X Mode, ϕ does not perturb the electric field; it only brings in additional elastic energy without generating other destabilizing torques. A factor influencing the development of ϕ cannot, therefore, lower the X threshold or widen the range of existence of the X Mode.

Figures 4 and 5 show that the phase boundaries of the X and Y Modes have the shapes found in figure 3 (*a*) even for weak anchoring. The effect of diminishing the anchoring strengths is strong when R_E is low and the sample sufficiently thin. The presence of K_{24} may dominate when $\mathbf{H}_\perp$ acts close to z [figures 4 (*e*) and 4 (*f*)]. The phase boundaries are determined in a thin sample for a few extreme sets of anchoring strengths (figure 6). While the wave vector of the X Mode tends to vanish on curve 2, the Y Mode wave vector generally remains non-zero on curve 1. For strong anchoring, the phase diagram closely resembles figure 3 (*a*), hence this case is left out. Diminution of polar anchoring strength tends to push the X phase boundary to lower α [compare figures 6 (*a*) and 6 (*b*)]. The effect of K_{24} in promoting the Y Mode in the low R_E range close to $\alpha = \pi/2$ can be appreciated from figures 6 (*c*) and 6 (*d*).

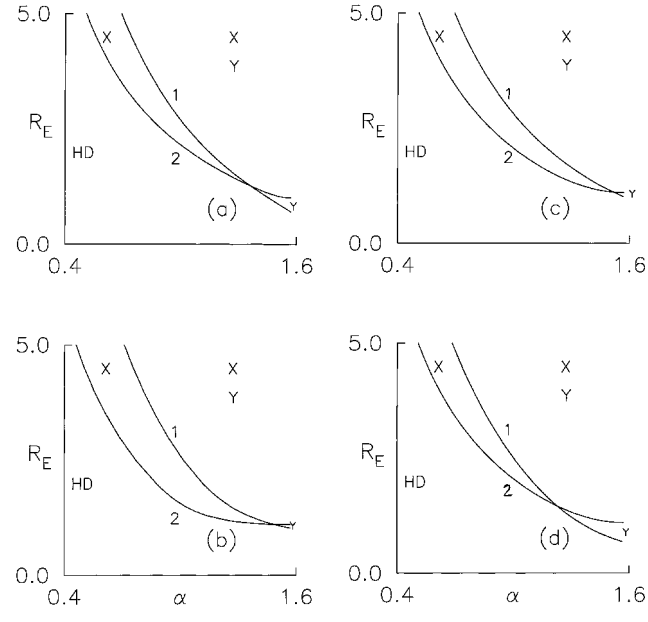

Figure 6. Phase boundaries for the Y (curve 1) and X (curve 2) Modes for a thin sample ($h = 2{\cdot}5\,\mu m$) when anchoring energy is finite (compare with figure 3). Parameters (10) for 5CB are employed. K_{24} is zero except in (*d*) where $K_{24} = 1{\cdot}5K_2$. The anchoring strengths take the values $(B_\theta, B_\phi) = (a)\ (10^{-2}, 10^{-6})$, $(b)\ (10^{-6}, 10^{-2})$, $(c, d)\ (10^{-6}, 10^{-6})\,erg\,cm^{-2}$. Comparisons of (*c*) and (*d*) shows that K_{24} can extend the domain of existence of the Y Mode when R_E is low (see § 4.2).

4.3. *Flexoelectricity with weak anchoring; qualitative discussion*

When flexoelectricity is included, terms $(e_1 + e_3)\psi_{,xz}$ and $(e_1 + e_3)\psi_{,xy}$ are added to the right-hand sides of U_θ

and U_ϕ, respectively, in equation (6); in addition, the following changes are made in (2)–(8):

$$f_F = e_1(\phi_{,y} + \theta_{,z})\psi_{,x} + e_3(\theta_{,x}\psi_{,z} + \phi_{,x}\psi_{,y}) + E_{xo}(e_1 + e_3)(\theta_{,x}\theta + \phi_{,x}\phi);$$
$$A_F = 4\pi(e_1 + e_3)(\phi_{,xy} + \theta_{,xz});$$
$$\tau_\theta = -e_1 E_{xo} + e_1\psi_{,x}; \quad \lambda_D = 4\pi e_3\theta_{,x} \qquad (21)$$

where e_1 and e_3 are the flexoelectric coefficients. Flexoelectricity has two important effects. At the level of the bulk equilibrium equations (3)–(5), it prevents perturbations from having definite spatial symmetry even when the rigid anchoring hypothesis is assumed. As the flexoelectric coefficients are $\sim 10^{-4}$ esu, this effect becomes prominent in a thick sample when E_{xo} is low enough (see § 5 of [20]). Flexoelectricity also enters the surface torque (7), (21) with one contribution being proportional to E_{xo} (see τ_θ). If the voltage is a.c. with sufficiently high frequency, the term $\sim E_{xo}$ in τ_θ averages to zero. When the voltage is d.c. and the anchoring weak, the above contribution causes HD to develop *without* threshold, however small the voltage—analogous to the effect discussed in [15]. For d.c. voltage, therefore, the analysis of § 2 to § 4 will not hold as the ground state will not remain aligned along x.

5. PD under E applied normal to the plates

The nematic is sandwiched between electrodes $z = \pm h$ to which a voltage V_z is applied. The sample is effectively infinite along x and y. Rigid director anchoring is assumed so that quantities associated with surface energy are ignored; K_{24} will cease to matter. Results can be scaled so as to be independent of sample thickness; hence some convenient value (say 100 μm) is assigned to h. In the absence of distortion,

$$\mathbf{E}_o = (0, 0, E_{zo}); \quad E_{zo} = V_z/2h.$$

Under deformation, $\mathbf{n}$ and $\mathbf{E}$ are again given by equation (1). In equation (3), the first term is replaced by $\varepsilon_A E_{zo}\theta_{,x}$. In (2), f_E is redefined,

$$f_E = -\frac{\varepsilon_A E_{zo}^2\theta^2}{8\pi} + \frac{\varepsilon_A E_{zo}\theta\psi_{,x}}{4\pi};$$

in (5), U_ϕ vanishes and in (4),

$$U_\theta = \frac{\varepsilon_A E_{zo}^2\theta}{4\pi} - \frac{\varepsilon_A E_{zo}\psi_{,x}}{4\pi}.$$

As $\mathbf{E}$ is normal to the surface of the conductor, the tangential components of $\mathbf{E}$ should vanish at the boundaries†; i.e. $\psi_{,x}$ and $\psi_{,y}$ should become zero at the plates. As we are interested in linear perturbations governed by linear equations, the x and y dependence is imposed of by the *ansatz* $\exp i(q_x x + q_y y)$ where q_x and q_y are independent of space variables. Then, the vanishing of the tangential components of $\mathbf{E}$ is ensured if ψ vanishes at the boundaries. Including the rigid anchoring hypothesis, expression (9) is replaced by

$$\theta = 0; \quad \phi = 0; \quad \psi = 0 \text{ at } z = \pm h \qquad (22)$$

for all varieties of deformations. In a formal analogy with the weak anchoring conditions for the director perturbations, we can regard the vanishing of ψ in (22) as the electric analogue of 'rigid anchoring' on ψ; similarly, the condition of the vanishing $\psi_{,z}$ in (9) for the other configuration can be said to be 'free anchoring' for ψ. Significantly, ψ affects only the X and XY Modes and neither HD nor the Y Mode in this geometry.

5.1. *H along symmetry directions; HD and X Modes*

First, the HD threshold is derived. Let $\mathbf{H}$ act along x or z; then ϕ becomes decoupled and damps out. When perturbations depend only on z, ψ is decoupled from θ and vanishes as per expression (22). In a nematic with $\varepsilon_A, \chi_A > 0$ (such as 5CB [18] or PBG [6]), $\mathbf{H}_\parallel$ stabilizes $\mathbf{n}_o$ against the action of $\mathbf{E}$ resulting in the electric splay threshold ($E_{zo} = E_1$) defined by

$$E_1^2 = \left(\frac{\pi^2}{4} + \frac{\chi_A h^2 H_\parallel^2}{K_1}\right)\frac{4\pi K_1}{\varepsilon_A h^2}. \qquad (23)$$

In a nematic (such as M1 [22]) with $\chi_A > 0$ and $\varepsilon_A < 0$, the magnetic splay threshold [$H_\perp = H_1$] is possible with $\mathbf{H}_\perp$ along z ($\alpha = \pi/2$):

$$H_1^2 = \left(\frac{\pi^2}{4} - \frac{\varepsilon_A E_{zo}^2 h^2}{4\pi K_1}\right)\frac{K_1}{\chi_A h^2}. \qquad (24)$$

For the same orientation of $\mathbf{H}_\perp$, the electric splay threshold in a nematic (such as CCH–7 [23]) with $\varepsilon_A > 0$ and $\chi_A < 0$ is $E_{zo} = E_2$ with

$$E_2^2 = \left(\frac{\pi^2}{4} - \frac{\chi_A h^2 H_\perp^2}{K_1}\right)\frac{4\pi K_1}{\varepsilon_A h^2}. \qquad (25)$$

For the X Mode, θ and ψ are out of phase along x; hence θ and $\psi_{,x}$ are in phase. While the z dependence of

† In a real situation, the electrodes may be covered with a layer of surfactant for the purpose of aligning the director. If the surfactant is also a conductor, then the boundary conditions will remain (22). If the surfactant is a dielectric (isotropic or anisotropic), interesting possibilities are raised. The present work does not address these complications.

θ brings in splay deformation, its x dependence introduces bend. Unless this additional elastic torque is compensated by a destabilizing influence, the X Mode cannot develop. The governing equations support two solutions of which we select the one with θ and ψ even, corresponding to the *ansatz*

$$(\theta, \psi) = \left[\theta_M \sin\left(\frac{Q_x x}{h}\right), \psi_M \cos\left(\frac{Q_x x}{h}\right)\right]\cos\left(\frac{\pi z}{2h}\right).$$

Depending upon the material, either $H_\perp$ or E_{zo} is expressed as a function of Q_x using the compatibility condition arising out of the governing equations. It can be analytically established that the X Mode threshold cannot exist in any of the three types of material since the neutral stability curve rises continuously from the corresponding HD threshold without showing a minimum when Q_x increases from zero.

The physical reason for this is not far to seek. The torque on θ arising from $\mathbf{E}'$ is $\sim \varepsilon_A E_{zo} \psi_{,x}$. In a material with $\varepsilon_A > 0$, for instance, $\psi_{,x}$ stabilizes the initial orientation adding to the existing stabilizing influence (of $\mathbf{H}_\parallel$ in 5CB or of $\mathbf{H}_\perp$ in CCH–7); this ensures the continuous rise of the neutral stability curve for the X Mode from the corresponding HD threshold—equations (23) or (25). Even in a material such as M1 with $\varepsilon_A < 0$, the destabilizing effect of $\psi_{,x}$ cannot overcome the additional stabilizing torque corresponding to the bend deformation. In this section, therefore, we do not study the X Mode.

5.2. *Y Mode in a material with positive susceptibility anisotropies*

The Y Mode can form in nematics with high elastic anisotropy [6, 8, 14]. As the Y Mode deformation does not perturb $\mathbf{E}_o$, ψ becomes decoupled from θ and ϕ. As the X Mode cannot exist, the XY Mode also is of no consequence; the XY threshold merely degenerates into the Y threshold with wave vector along y. Hence, only the Y Mode is studied.

The well known results for materials with positive susceptibility anisotropies [6, 8, 14] are summarized for comparison with results of § 3.1. We initially select $\mathbf{H}_\parallel$ which has a stabilizing influence on both θ and ϕ. The Y Mode deformation conforms to either SOLUTION 1 or SOLUTION 2 of § 3.1 (with ψ being ignored); the Y threshold is determined as described in earlier sections. With the *ansantz*

$$(\theta, \phi) = \left[\theta_1(\xi)\cos\frac{Q_y y}{h}, \phi_1(\xi)\sin\frac{Q_y y}{h}\right]; \quad \xi = \frac{z}{h},$$

the governing equations take the form

$$\phi_{1,\xi\xi} - \left(\frac{\pi^2}{4} r_N^2 + k_{12} Q_y^2\right)\phi_1 - (k_{12} - 1) Q_y \theta_{1,\xi} = 0;$$
$$\theta_{1,\xi\xi} + \left(\zeta - \frac{Q_y^2}{k_{12}}\right)\theta_1 + \left(1 - \frac{1}{k_{12}}\right) Q_y \phi_{1,\xi} = 0; \tag{26}$$

where θ_1 and ϕ_1 vanish at the boundaries and

$$r_N = \frac{H_\parallel}{H_2}; \quad H_2 = \frac{\pi}{2h}\left(\frac{K_2}{\chi_A}\right)^{1/2}; \quad k_{12} = \frac{K_1}{K_2};$$
$$\zeta = \frac{\pi^2}{4} R_E^2 + \frac{\chi_A h^2 H_\parallel^2}{K_1}(R_E^2 - 1); \quad R_E = \frac{E_{zo}}{E_1}. \tag{27}$$

The solution of (26) at a given k_{12} and weak $\mathbf{H}_\parallel$ results in a neutral stability curve which expresses ζ as a function of Q_y. The minimum ζ_P occurring at $Q_y = Q_P$ corresponds to the electric Y Mode threshold $E_P = E_{zo}(Q_P)$. The reduced electric Y threshold $R_Y = E_P/E_1$ and threshold wave vector, Q_P, can be studied as functions of k_{12} and $H_\parallel$.

Figures 7 (*a–c*) contain results for the Y Mode. As individual values of $\varepsilon_\parallel$ and $\varepsilon_\perp$ are unimportant, a convenient value (say, 5) is assigned to ε_A; similarly, $\chi_A = 10^{-7}$ emu. When r_N is low, R_Y decreases (and Q_P increases) with increasing k_{12}; the higher the k_{12}, the more favourable the Y Mode compared with HD. Sufficient increase of r_N causes the Y Mode to become quenched. At a given k_{12}, $R_Y \to 1$ and $Q_P \to 0$ when $r_N \to r_{NC}$ so that for $r_N > r_{NC}$, only HD exists. Clearly, r_{NC} increases with k_{12}.

A qualitative explanation can be given for some of the results. HD is associated only with θ on which $\mathbf{H}_\parallel$ exerts a stabilizing influence. This causes the HD threshold, equation (23), to increase with $H_\parallel$. When $\mathbf{H}_\parallel$ is absent and k_{12} is high enough, the Y Mode sets in with θ and ϕ instead of HD, because the Y Mode has lower total free energy than HD. But $\mathbf{H}_\parallel$ has a stabilizing influence on both θ and ϕ of which the existence of the latter is central to the formation of the Y Mode. When $\mathbf{H}_\parallel$ is strong enough, its stabilizing action on ϕ makes the development of the Y Mode with non-zero wave vector impossible.

These results, shown in figures 7 (*a*) and 7 (*b*), can be qualitatively compared with those of § 3.1, curves 3 in figures 1 (*a*) and 1 (*b*). In both cases, the material has positive susceptibility anisotropies. When $\mathbf{E}_o$ acts along $\mathbf{n}_o$, the magnetically induced Y Mode survives for all E_{xo}. This is because the Y Mode distortions perturb the electric field and $\mathbf{E}'$ causes additional destabilizing torques whose magnitude increases with E_{xo}. In the present case, the Y Mode deformations cause no perturbation of the electric field; as indicated above,

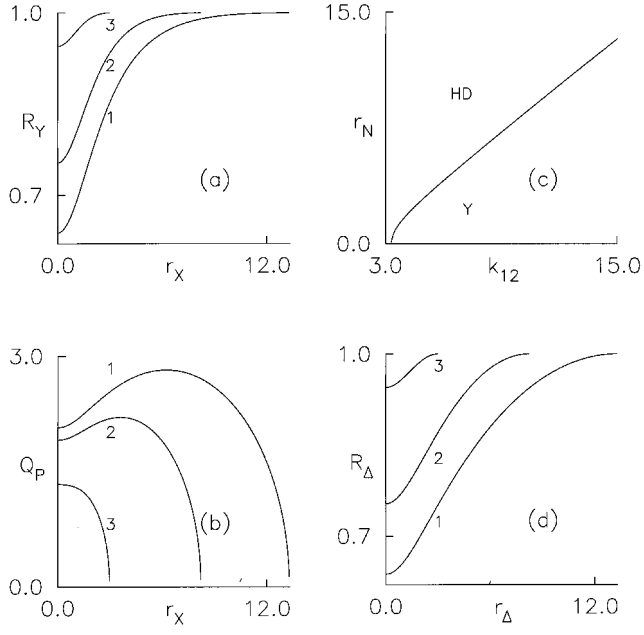

Figure 7. (*a–c*) Results for the Y Mode in high elastic anisotropy nematics with positive susceptibility anisotropies (see § 5.2 for definitions). The elastic ratio $k_{12}=K_1/K_2$. The Y Mode is induced in the planar oriented sample by applying a voltage between the plates $z=\pm h$. $\mathbf{H}_\parallel$ along x stabilizes the initial orientation. Rigid anchoring hypothesis is employed. In (*a*) and (*b*), curves are drawn for $k_{12}=$(1) 15, (2) 10, (3) 5. The reduced electric threshold and dimensionless wave vector are plotted as functions of the reduced stabilizing magnetic strength in (*a*) and (*b*), respectively. (*c*) r_N is the reduced stabilizing magnetic strength, equation (28), necessary to quench the Y Mode for a given k_{12}. The diagrams (*b*) and (*c*) also serve to represent results for a material having $\varepsilon_A>0$ and $\chi_A<0$ with the stabilizing $\mathbf{H}_\perp$ acting along y. Relevant quantities are redefined as in § 5.3. The variation of R_Δ, the reduced electric Y threshold, versus the dimensionless stabilizing magnetic strength, r_Δ, is shown in figure 7 (*d*).

the electrically induced Y Mode is suppressed by a sufficiently strong $\mathbf{H}_\parallel$.

An estimate of r_{NC} can be made using the approach of [30]. Briefly, this involves solving the governing equations of the Y Mode with boundary conditions (22). Substituting for θ and ϕ, the total free energy F is expanded in powers of Q_y; up to lowest order, $F=N_o+N_1Q_y^2$. Using equation (23), N_o is found to vanish. The critical point between the Y Mode and HD is found from $N_1=0$ which reduces to

$$\left[\frac{\pi^2}{4}(k_{12}-2)k_{12}-j^2\right]\left(j^2+\frac{\pi^2}{4}\right)\left(\frac{\tanh j}{j}\right)-\frac{(k_{12}-1)^2\pi^2}{2}=0;$$

$$j=\frac{r_N\pi}{2}. \qquad (28)$$

Solving (28) numerically, r_{NC} is obtained as a function of k_{12} [figure 7 (*c*)]. Clearly, r_{NC} increases with k_{12}. Putting $j=0$ in (28) results in

$$k_{12}=k_C; \quad k_C=1+\frac{\pi}{(\pi^2-8)^{1/2}}. \qquad (29)$$

This is the well known result [6, 8, 14] that the Y Mode can occur only in a material with $k_{12}>k_C$; the limit k_C is the point of intersection of the phase boundary with the k_{12} axis in figure 7 (*c*). When $k_{12}\gg1$ (very high elastic anisotropy), the stabilizing $\mathbf{H}_\parallel$ required to quench the Y Mode is also very strong; then, $j\gg1$ and $\tanh j\approx1$. In this limit, (28) reduces to $r_{NC}\approx k_{12}$ which yields the almost straight segment of the phase boundary with unit slope in the high k_{12} limit in figure 7 (*c*).

5.3. *Y Mode with $\varepsilon_A>0$ and $\chi_A<0$; $\alpha=0$*

$\mathbf{H}_\perp$ acts along y and has a stabilizing influence on ϕ; $\mathbf{H}_\perp$ does not directly couple with θ. Hence, the Y Mode should become quenched if $\mathbf{H}_\perp$ is strong enough. The governing equations can be cast into the form (26) with the redefinitions

$$r_N=r_\Delta=\frac{H_\perp}{H_2}; \quad H_2=\frac{\pi}{2h}\left(-\frac{K_2}{\chi_A}\right)^{1/2};$$
$$\zeta=\frac{\pi^2}{4}R_e^2; \quad R_e=\frac{E_{zo}}{E_S}; \quad E_S^2=\frac{K_1\pi^3}{\varepsilon_A h^2}. \qquad (30)$$

At given values of r_Δ and k_{12}, the reduced Y threshold is $R_e=R_\Delta$ at the wave vector Q_P. For purposes of computation, $\chi_A=-10^{-7}$ emu and $\varepsilon_A=5$. As the solution of equation (26) determines the minimum ζ_P of ζ as a function of Q_y at given r_N and k_{12}, the Q_P versus r_Δ curves become identical to the Q_P versus r_N curves of § 5.2, figure 7 (*b*). As the critical point is determined in the limit of the vanishing wave vector, the phase boundary between the Y Mode and HD will be again given by figure 7 (*c*) with a suitable redefinition. Using the approach of [30] this conjecture can be shown to be true if we replace r_N of equations (27) and (28) by r_Δ of (30). The only difference lies in the plots of R_Δ versus r_Δ, figure 7 (*d*). At a given k_{12}, corresponding curves in figures 7 (*a*) and 7 (*d*) coincide only at the critical point and at zero stabilizing magnetic field. At other points, $R_\Delta<R_Y$. This can be explained by comparing the values of ζ_P (Y threshold) at a given k_{12}. From equations (30) and (27),

$$R_\Delta^2=R_Y^2+\frac{\chi_A h^2 H_\parallel^2}{K_1}(R_Y^2-1)\frac{4}{\pi^2}; \quad \chi_A>0.$$

Clearly, R_Δ and R_Y coincide when $H_\parallel$ vanishes and also when R_Y equals unity. As $R_Y\leqslant1$, $R_\Delta\leqslant R_Y$ at general values of the stabilizing magnetic field.

5.4. *Y Mode with $\varepsilon_A > 0$ and $\chi_A < 0$; $\alpha = \pi/2$*

$\mathbf{H}_\perp$ (acting along z) has a stabilizing influence on θ but no direct coupling with ϕ. The electric splay threshold is E_2, equation (25). Using the method of [30], the Y Mode is found to occur only if $k_{12} > k_C$ of (29). As in §5.2, we solve (26) to calculate the Y threshold $E_P = E_{zo}(Q_P)$ except that now

$$\zeta = \left(\frac{E_{zo}\pi}{E_2\ 2}\right)^2 + \frac{\chi_A h^2 H_\perp^2}{K_1}\left(1 - \frac{E_{zo}^2}{E_2^2}\right).$$

The reduced Y threshold $R_2 = E_P/E_2$. For a given $k_{12} > k_C$, the wave vector Q_P does not vary with increasing $H_\perp$. Hence, the Y Mode cannot be quenched by increasing the strength of the stabilizing $\mathbf{H}_\perp$ impressed along z. When $H_\perp = 0$, $R_2 = R_o$ and $R_o < 1$. When $H_\perp$ is increased, R_2 increases from R_o. When $\mathbf{H}_\perp$ is very strong, R_2 asymptotically approaches (but stays below) unity. This is clear from the discussion of §5.3. At a given k_{12}, the minimum ζ_P occurring at wave vector Q_P has a unique value. In the present case, the reduced Y threshold has different values for zero and non-zero $H_\perp$. Clearly,

$$R_o^2 = R_2^2 + \frac{\chi_A h^2 H_\perp^2}{K_1}(1 - R_2^2)\frac{4}{\pi^2}; \quad \chi_A < 0.$$

As $R_2 \leqslant 1$, $R_o \leqslant R_2$. R_o and R_2 coincide in value when the stabilizing $\mathbf{H}_\perp$ is absent for any $k_{12} > k_C$. R_o and R_2 both attain unity at $k_{12} = k_C$ regardless of the strength of $\mathbf{H}_\perp$ acting along z. As R_o is independent of $H_\perp$, differentiation shows that $\partial R_2/\partial H_\perp > 0$ showing that R_2 increases with $H_\perp$.

5.5. *Y Mode with $\varepsilon_A < 0$ and $\chi_A > 0$; $\alpha = \pi/2$*

The magnetically induced Y Mode is studied exactly as in §5.4. Under the stabilizing action of $\mathbf{E}_o$ acting along z, the HD threshold is H_1 of equation (24). The governing equations can be obtained from (26) by putting $r_N = 0$ and redefining

$$\zeta = \frac{\varepsilon_A h^2 E_{zo}^2}{4\pi K_1}\left(1 - \frac{H_\perp^2}{H_1^2}\right) + \frac{H_\perp^2}{H_1^2}\frac{\pi^2}{4}.$$

Following [30], the critical point calculation shows again that the Y Mode is possible provided that $k_{12} > k_C$ of (29). As before, the minimum ζ_P of ζ occurring at a given $Q_y = Q_P$ depends only on k_{12}; hence Q_P is independent of E_{zo}. At a given E_{zo}, ζ_P corresponds to the reduced magnetic threshold $r_P = H_\perp(Q_P)/H_1$. If r_o is the reduced magnetic threshold at $E_{zo} = 0$,

$$r_o^2 = \frac{\varepsilon_A h^2 E_{zo}^2}{4\pi K_1}(1 - r_P^2)\frac{4}{\pi^2} + r_P^2; \quad \varepsilon_A < 0.$$

As $r_P \leqslant 1$, $r_o \leqslant r_P$. Suppose E_{zo} is increased from zero at a given k_{12}. Then, r_P increases from r_o tending asymptotically to (but remaining less than) unity when E_{zo} attains high values. Again, $\partial r_P/\partial E_{zo} > 0$ as r_o is independent of E_{zo}; i.e. r_P increases with E_{zo}.

5.6. *General orientations of $\mathbf{H}_\perp$ in the yz plane; opposite susceptibility anisotropies*

In §5.3–§5.5, $\mathbf{H}_\perp$ is assumed to act exactly along a symmetry direction. Such a situation may not be realizable in an experiment. The results of §3 and §4 also create interest in a study of the effects of an oblique $\mathbf{H}_\perp$ on the Y Mode.

In a material with $\chi_A < 0$ and $\varepsilon_A > 0$, $\mathbf{E}_o$ along z destabilizes and $\mathbf{H}_\perp$ in the yz plane stabilizes $\mathbf{n}_o$. As $\mathbf{H}_\perp$ acts obliquely in the yz plane, θ and ϕ become coupled. The initial task is to fix the HD threshold. With dependence on z, the governing equations support two uncoupled solutions; we choose the one with θ and ϕ symmetric. Using conditions (22), the α dependent electric HD threshold is given by

$$E_F^2 = \frac{\pi^3[K_1 K_2 \pi^2 - 4\chi_A h^2 H_\perp^2 (K_1 C_\alpha^2 + K_2 S_\alpha^2)]}{\varepsilon_A h^2 (K_2 \pi^2 - 4\chi_A h^2 H_\perp^2 C_\alpha^2)}. \tag{31}$$

When $\alpha = \pi/2$, E_F of (31) reduces to E_2 of (25). In this case, ϕ damps out and θ is influenced by $\mathbf{E}_o$ and $\mathbf{H}_\perp$. In the opposite limit of $\alpha = 0$, ϕ again damps out. As θ now couples only to the destabilizing $\mathbf{E}_o$ along z, E_F reduces to the usual splay electric threshold E_S of (30).

Similarly, in a material with $\chi_A > 0$ and $\varepsilon_A < 0$, the magnetic HD threshold under the stabilizing action of $\mathbf{E}_o$ is α dependent:

$$H_F^2 = \frac{K_2 \pi^2 (K_1 \pi^3 - \varepsilon_A h^2 E_{zo}^2)}{4\chi_A h^2 [\pi^3 (K_1 C_\alpha^2 + K_2 S_\alpha^2) - \varepsilon_A h^2 E_{zo}^2 C_\alpha^2]}. \tag{32}$$

When $\alpha = \pi/2$, ϕ becomes decoupled and (32) reduces to H_1 of (24). When $\alpha = 0$, θ damps out; ϕ becomes coupled to $\mathbf{H}_\perp$ acting along y so that (32) reduces to the magnetic twist threshold.

The Y Mode threshold calculation is not straightforward. Due to the presence of the magnetic cross coupling terms, θ and ϕ become linear superpositions of components that are out of phase along y (§3.2); while one component conforms to SOLUTION 1, the other conforms to SOLUTION 2 (§3.1). As HD has pure spatial symmetry, the Y Mode and HD cannot meet at a true critical point. When the Y and HD thresholds become equal, Q_P may not be zero.

5.7. *Y Mode in a material with $\varepsilon_A > 0$ and $\chi_A < 0$; $\mathbf{H}_\perp$ in the yz plane*

As seen from §5.3 and §5.4, the actions of $\mathbf{H}_\perp$ at the two extremities of the α range are quite different. When $\mathbf{H}_\perp$ of arbitrary strength is directed along z, it does not

affect the occurrence of the Y Mode. If $\mathbf{H}_\perp$ acts along y, it can suppress the Y Mode at a critical point. In both cases, the distortions have definite spatial symmetry. Once α is changed to a general value, this symmetry no longer holds. The changeover from Y Mode to HD under increase of $H_\perp$ should be discontinuous, in general. Still, one can anticipate that when α is in the neighbourhood of zero, the discontinuity should be less, as a critical point exists at $\alpha = 0$. Similarly, the non-existence of a critical point at $\alpha = \pi/2$ implies that the suppression of the Y Mode should becomes more discontinuous when α is close to $\pi/2$. Hence, the effect of varying α (at a given $H_\perp$) and $H_\perp$ (at a given α) should prove interesting. The reduced Y threshold is defined in terms of E_F, equation (31), as $R_E = E_{zo}/E_F$. The reduced stabilizing magnetic strength is defined in terms of the twist magnetic threshold H_2 of (30): $r_H = H_\perp/H_2$. For purposes of computation, convenient values for some of the parameters (say, $h = 0{\cdot}01$ cm, $\chi_A = -10^{-7}$ emu and $\varepsilon_A = 5$) are used.

Figures 8 (a–d) contain plots of R_E versus r_H for different α for one material (k_{12}). At a given α, increase of r_H above some r_C causes the Y Mode to disappear when $\mathbf{H}_\perp$ becomes sufficiently strong. But the discontinuity of changeover from Y Mode to HD is much less when $\mathbf{H}_\perp$ acts closer to y [figures 8 (c) and 8 (d); the transition appears to be almost continuous] than when $\mathbf{H}_\perp$ is directed nearer to z [figures 8 (a) and 8 (b)]; in the latter case, we take r_C to be the value of r_H at which $R_E = 1$, though Q_P is non-zero. When α is small, r_C diminishes when α takes increasing values [figures 8 (c) and 8 (d)]. In the opposite limit [figures 8 (a) and 8 (b)], r_C diminishes sharply when α is decreased even slightly from $\pi/2$. This indicates the shape of the phase boundary between the Y Mode and HD [figures 8 (e) and 8 (f)].

At a given α, r_C is the value of r_H at which R_E equals unity; r_C is plotted against α. The phase boundary has the same shape for the chosen k_{12} values but the region of existence of the Y Mode expands with increase of k_{12}. The phase diagrams in the range $\pi/2 \leqslant \alpha \leqslant \pi$ can be obtained by reflecting figures 8 (e) and 8 (f) in the line $\alpha = \pi/2$. While r_C tends to a finite limit at $\alpha = 0$, it diverges when $\alpha \longrightarrow \pi/2$ in agreement with the results of § 5.3 and § 5.4. The valley in the mid-range is due to the presence of a larger portion of SOLUTION 2 in the distortions; in this region the Y Mode is suppressed by even moderately strong stabilizing $\mathbf{H}_\perp$.

Three distinct regions are discernible in figures 8 (e) and 8 (f). In illustration, consider figure 8 (e). The line $r_C = 1$ (weak stabilizing $\mathbf{H}_\perp$) does not cut the phase boundary; here, only the Y Mode exists. The line $r_C = 9$ (strong $\mathbf{H}_\perp$) cuts the phase boundary only close to $\alpha = \pi/2$. Here, only HD exists over the entire region except close to $\alpha = \pi/2$ where the Y Mode prevails. The intermediate line $r_C = 4$ has two intercepts. As α is increased from zero, we have the Y Mode, then HD and again the Y Mode (though over a narrow α range). HD (the high symmetry phase) occurs in a 're-entrant' way when α is increased from zero (or diminished from $\pi/2$).

The above conclusions are reinforced by figure 9 which contains α variations of R_E and Q_P. At a given, moderate, r_H, figures 9 (a) and 9 (b), k_{12} plays an important role in determining the range of existence of the Y Mode. When k_{12} is high (curve 1), the Y Mode prevails

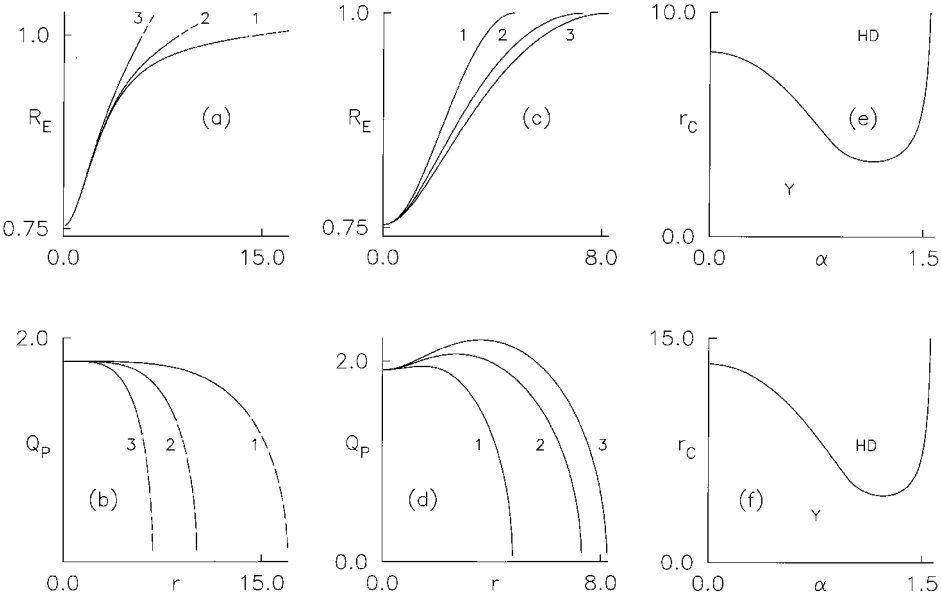

Figure 8. Y Mode in high elastic anisotropy nematics with positive dielectric and negative diamagnetic anisotropies. $\mathbf{H}_\perp$ acting in the yz plane has stabilizing action at general α. The reduced electric Y threshold (R_E) and stabilizing magnetic strength (r_H) are defined in § 5.7; Q_P is the dimensionless wave vector. $k_{12} = 10$ in (a–d). Curves are drawn for $\alpha = (1)$ 1·56, (2) 1·54, (3) 1·5 rad in (a, b) and for $\alpha = (1)$ 0·78, (2) 0·39, (3) 0·01 rad in (c, d). r_C is in the r_H at which the Y Mode and HD thresholds are equal. Plots of r_C versus α for $k_{12} =$ (e) 10, (f) 15. Y and HD mark, respectively, the regions of existence of these distortions. The 're-entrant' occurrence of HD at moderately strong $\mathbf{H}_\perp$ should be noted.

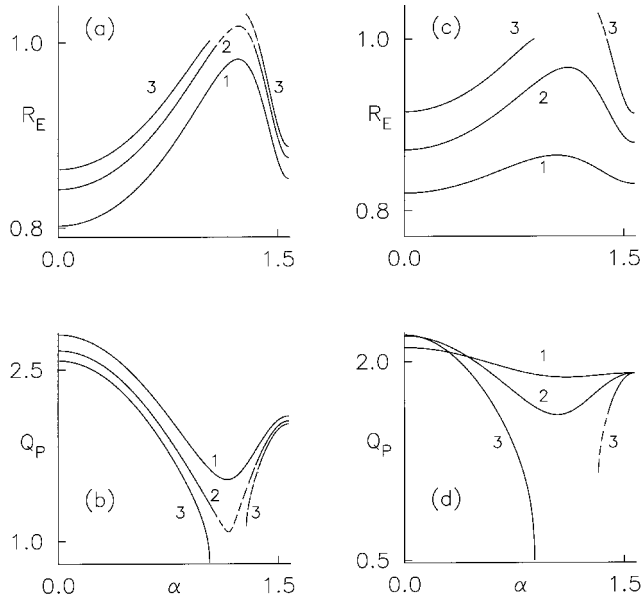

Figure 9. Details as in figure 8 except that R_E and Q_P are functions of magnetic tilt, α (see § 5.7). The existence of the re-entrant HD depends critically on k_{12} and r_H. In (a, b), the reduced stabilizing magnetic strength, $r_H = 4{\cdot}5$ and $k_{12} = (1)\ 16, (2)\ 14, (3)\ 13$. In (c, d), $k_{12} = 10$ and $r_H = (1)\ 2, (2)\ 3, (3)\ 4$.

over the entire α range. At lower k_{12}, the re-entrant HD appears; the lower the k_{12}, the wider the range of HD. For a given material, figures 9 (*c*) and 9 (*d*), increase in r_H causes the appearance of HD in the intermediate α range. At each point, the change between HD and the Y Mode occurs discontinuously. When k_{12} is sufficiently low or r_H high enough (curves 3), the Y Mode does not even exist as a solution in the intermediate α range.

5.8. *Y Mode in a material with $\varepsilon_A < 0$ and $\chi_A > 0$; $\mathbf{H}_\perp$ in the yz plane*

As seen from § 5.5, $\mathbf{E}_o$ acting along z cannot suppress the Y Mode in a material with $k_{12} > k_C$; the Y Mode is also described by deformations with pure spatial symmetry. If $\mathbf{H}_\perp$ is directed along y, HD sets in above the twist magnetic threshold with $\mathbf{E}_o$ having no effect on ϕ. Hence, the Y Mode should be suppressed if α is diminished sufficiently from $\pi/2$. At general α, the Y Mode perturbations do not have pure spatial symmetry and the solution is effected as in § 5.7. The transition between the Y Mode and HD is discontinuous with respect to Q_P. Due to the direct coupling of $\mathbf{E}_o$ with θ, the value of α demarcating the phase boundary will depend on E_{zo}. H_F of equation (32) is used to define the reduced magnetic Y threshold $r_H = H_\perp / H_F$; the reduced stabilizing electric field strength is defined in terms of the effective electric splay threshold, E_s:

$$R_E = \frac{E_{zo}}{E_s}; \quad E_s^2 = -\frac{K_1 \pi^3}{\varepsilon_A h^2}.$$

Figures 10 (*a*) and 10 (*b*) show the variation of threshold parameters with R_E at three α values close to $\pi/2$ for one material. The Y Mode is quenched when the stabilizing electric field strength is strong enough. Even a small variation of magnetic tilt from $\pi/2$ causes the Y Mode to disappear at low R_E. But the R_E necessary to quench the Y Mode is infinite at exactly $\alpha = \pi/2$ (§ 5.5). At $\alpha = \pi/2$, Q_P remains unchanged and $r_H < 1$ at all R_E. Results for α variation support the above conclusions (these are not shown). The cut-off value of α necessary to quench the Y Mode decreases (i.e. the α range of the Y Mode expands) when k_{12} is increased at a given R_E. With k_{12} fixed, the Y Mode is quenched at a higher α when R_E is increased.

Figures 10 (*c*) and 10 (*d*) contain phase diagrams for two materials. Increase of k_{12} widens the region of existence of the Y Mode in the R_E–α plane. These diagrams should be compared with curve 1 of figure 3 (*b*) (which is drawn for a material with positive susceptibility anisotropies with $\mathbf{E}_o$ impressed along x and $\mathbf{H}_\perp$ in the yz plane). The shapes of the two phase boundaries

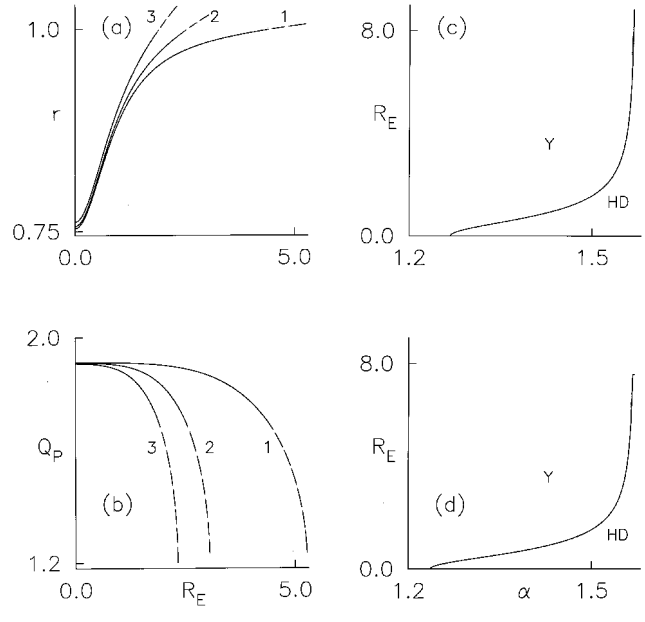

Figure 10. Y Mode in high elastic anisotropy nematic with negative dielectric and positive diamagnetic anisotropies. $k_{12} = 10$; the reduced magnetic Y threshold r_H and the reduced stabilizing electric strength R_E are defined in § 5.8. In (*a*) and (*b*), curves are drawn for $\alpha = (1)\ 1{\cdot}56, (2)\ 1{\cdot}54, (3)\ 1{\cdot}52$ rad. In (*c*) and (*d*), the critical R_E necessary to quench the Y Mode is plotted as a function of α for two materials with $k_{12} = (c)\ 10, (d)\ 15$. Compare (*c*) or (*d*) with curve 1 of figure 3 (*b*).

are similar except that one is obtained from the other through a reflection in a vertical line.

6. PD under E applied along *y*

This configuration is similar to that studied in § 2–§ 4 except that the electrodes are assumed to be at $y = \pm g$ with $2g \gg 2h$. In the absence of deformation,

$$\mathbf{E}_o = (0, E_{yo}, 0); \quad E_{yo} = V_Y/2g.$$

Under distortion, **n** and **E** are again given by equation (1). In (3), the first term is replaced by $\varepsilon_A E_{yo} \phi_{,x}$. In (2), f_E is redefined to be

$$f_E = \frac{\varepsilon_A E_{yo}}{4\pi} \phi \psi_{,x} - \frac{\varepsilon_A E_{yo}^2}{8\pi} \phi^2;$$

in (4), U_θ vanishes and in (5),

$$U_\phi = \frac{\varepsilon_A E_{yo}^2}{4\pi} \phi - \frac{\varepsilon_A E_{yo}}{4\pi} \psi_{,x}.$$

Rigid anchoring hypothesis is assumed. When perturbations depend only on z, ψ becomes decoupled from θ and ϕ. In a material with $\varepsilon_A < 0$ and $\chi_A > 0$, the magnetic HD threshold is

$$H_G^2 = \frac{K_1 \pi^2 (K_2 \pi^3 - \varepsilon_A h^2 E_{yo}^2)}{4\chi_A h^2 [\pi^3 (K_1 C_\alpha^2 + K_2 S_\alpha^2) - \varepsilon_A h^2 E_{yo}^2 S_\alpha^2]}. \quad (33)$$

When $\mathbf{H}_\perp$ acts along z, ϕ becomes damped out. As $\mathbf{E}_o$ acts along y, θ is coupled only to $\mathbf{H}_\perp$ so that (33) reduces to the magnetic splay threshold. When $\alpha = 0$, θ damps out and

$$H_G^2(\alpha = 0) = \frac{K_2}{\chi_A h^2} \left(\frac{\pi^2}{4} - \frac{\varepsilon_A h^2 E_{yo}^2}{4\pi K_2} \right),$$

with a twist appearing under the stabilizing action of $\mathbf{E}_o$ and destabilizing action of $\mathbf{H}_\perp$.

In a material with $\chi_A < 0$ and $\varepsilon_A > 0$, the electric HD threshold is

$$E_G^2 = \frac{\pi^3 [K_1 K_2 \pi^2 - 4\chi_A h^2 H_\perp^2 (K_1 C_\alpha^2 + K_2 S_\alpha^2)]}{\varepsilon_A h^2 (K_1 \pi^2 - 4\chi_A h^2 H_\perp^2 S_\alpha^2)}. \quad (34)$$

When $\alpha = \pi/2$, θ gets decoupled from ϕ and (34) reduces to the electric twist threshold. When $\mathbf{H}_\perp$ is directed along y, a twist distortion appears above the threshold

$$E_G^2(\alpha = 0) = \frac{4\pi K_2}{\varepsilon_A h^2} \left(\frac{\pi^2}{4} - \frac{\chi_A h^2 H_\perp^2}{K_2} \right)$$

under the joint actions of stabilizing $\mathbf{H}_\perp$ and destabilizing $\mathbf{E}_o$.

Out of the three PD Modes, the Y Mode does not involve ψ. The X Mode can be shown not to exist in materials with $k_{12} > 1$ as the neutral stability curve increases continuously with wave vector, exhibiting no minimum. This is clear from the governing equations as $\psi_{,x}$ is the only electric perturbation entering the torque equations. In a material with $\varepsilon_A > 0$, $\psi_{,x}$ has only a stabilizing influence. Even for $\varepsilon_A < 0$, the destabilizing effect of $\psi_{,x}$ is not strong as $\psi_{,x}$ is out of phase with ϕ along x, the direction of periodicity. Hence, neither the X nor the XY Modes are studied here.

6.1. *Y Mode in materials with $\varepsilon_A < 0$ and $\chi_A > 0$*

When $\mathbf{H}_\perp$ acts along z, HD involves only θ and occurs at the splay Fréedericksz threshold, H_S. As θ does not couple with $\mathbf{E}_o$, the HD threshold is independent of E_{yo}. In materials with high elastic anisotropy, the Y Mode (SOLUTION 1) can set in if $k_{12} > k_C$ of equation (29). In the present case, $\mathbf{E}_o$ has a stabilizing influence on ϕ and exerts no direct torque on θ. The governing equations can be recast into the form (26) with r_N replaced by R_E where

$$R_E = \frac{E_{yo}}{E_T}; \quad E_T = \frac{\pi}{2h} \left(-\frac{4\pi K_2}{\varepsilon_A} \right)^{1/2};$$

$$\zeta = \left(\frac{\pi H_\perp}{2H_S} \right)^2; \quad H_S = \frac{\pi}{2h} \left(\frac{K_1}{\chi_A} \right)^{1/2}.$$

Clearly, E_T is the equivalent electric twist Fréedericksz threshold. Plots of threshold parameters as functions of R_E are similar to those in figures 7 (*a*) and 7 (*b*). The phase boundary is defined by (28), figure 7 (*c*), where R_{EC} replaces r_{NC}.

With $\mathbf{H}_\perp$ in the yz plane, the results are more interesting. The Y Mode is now a superposition of SOLUTIONs 1 and 2. The reduced Y threshold, $r_H = H_\perp/H_G$, is defined in terms of H_G, equation (33), while the reduced stabilizing electric field, R_E, is defined in terms of E_T as above. The material chosen has $k_{12} = 10$. In the absence of $\mathbf{E}_o$, the Y Mode is suppressed if $\alpha < \alpha_C$; $\alpha_C \approx 1{\cdot}27$ rad. When E_{yo} is increased from zero, the Y Mode is quenched at sufficiently high R_E [figures 11 (*a–d*)]. Regardless of α, the Y Mode is quenched at the same R_E. In the low R_E range, however, increase of R_E actually appears to favour the Y Mode with r_H decreasing and Q_P increasing. This variation becomes pronounced when $\alpha > \alpha_C$ [figures 11 (*c*) and 11 (*d*)]. Although HD prevails at low R_E, the subsequent decrease in r_H actually causes the Y Mode to make a 're-entrant' appearance before being quenched again.

A possible reason for this is that θ does not get influenced directly by the stabilizing action of $\mathbf{E}_o$. When E_{yo} is high enough, the damping it imposes on ϕ is sufficient to quench the Y Mode even though θ is not directly affected by $\mathbf{E}_o$. When E_{yo} is low, however, its stabilizing influence on ϕ may be partly overcome by $\mathbf{H}_\perp$ provided that $\mathbf{H}_\perp$ acts sufficiently close to y. At low α, $\mathbf{H}_\perp$ also exerts a weak destabilizing torque which may

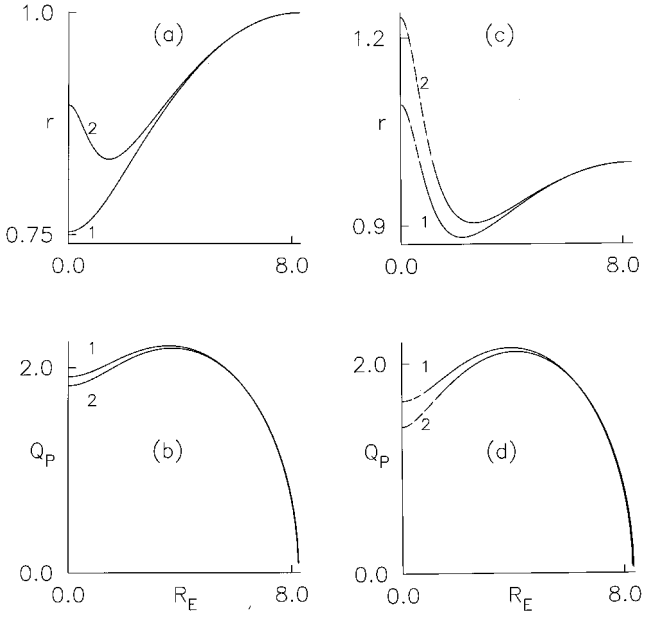

Figure 11. Plots of Y Mode threshold parameters in a material with $\varepsilon_A < 0$ and $\chi_A > 0$. $\mathbf{E}_o$ along y has a stabilizing influence while $\mathbf{H}_\perp$ in the yz plane destabilizes $\mathbf{n}_o$. $k_{12} = 10$. The dimensionless Y threshold, r_H and the reduced electric strength, R_E are defined in § 6.1. In (*a*) and (*b*), curves are drawn for $\alpha = (1)\ 1{\cdot}57$, (2) 1·35 rad. In (*c*) and (*d*), $\alpha = (1)\ 1{\cdot}2$, (2) 1·1 rad. An increase in R_E causes the Y Mode to appear in the 're-entrant' way (*c*, *d*). At sufficiently high R_E, the Y Mode is quenched.

help θ to develop. As θ is not directly damped by $\mathbf{E}_o$, the Y Mode may actually show a revival. The α variation (figure 12) complements the results of figure 11 and also indicates the shape of the phase boundary. As R_E increases, the α necessary to quench the Y Mode diminishes. The transition between the Y Mode and HD is discontinuous but the degree of discontinuity becomes less when R_E is high enough [compare figures 12 (*a*) and 12 (*b*) with 12 (*c*) and 12 (*d*)]. The transition points also come closer when R_E is sufficiently high [figures 12 (*c*) and 12 (*d*)].

Not surprisingly, the phase boundary takes the form shown in figure 12 (*e*) and 12 (*f*), bearing a striking resemblance to the phase boundaries derived elsewhere for a homeotropic sample (see figure 1 of [21]; a reflection in the α axis is needed before comparison) as well as some in this work [see figures 8 (*e*) and 8 (*f*)]. The higher the k_{12}, the wider the region of existence of the Y Mode. The vertical intersection of the phase boundary with the α axis occurs at α_C for the given material; the phase boundary again becomes vertical at $\alpha_o < \alpha_C$. By drawing vertical lines at different α, three distinct regions can be recognized: at $\pi/2 > \alpha > \alpha_C$, the Y Mode exists at low R_E and is quenched when R_E takes sufficiently high values; at $\alpha_o < \alpha < \alpha_C$, the Y Mode appears re-entrantly between HD; at $0 < \alpha < \alpha_o$, only HD prevails.

7. Conclusions

Static PD thresholds have been studied when **H** and $\mathbf{E}_o$ act simultaneously on a planar nematic sample with $\mathbf{n}_o$ along x; the direction of periodicity is along x (X Mode) or along y (Y Mode). In the main, the rigid anchoring hypothesis has been utilized, along with linear perturbation analysis; in one case, the anchoring is assumed to be weak. Choice of different susceptibility anisotropies as well as symmetry directions for $\mathbf{E}_o$ leads to a variety of phase diagrams for the distortions.

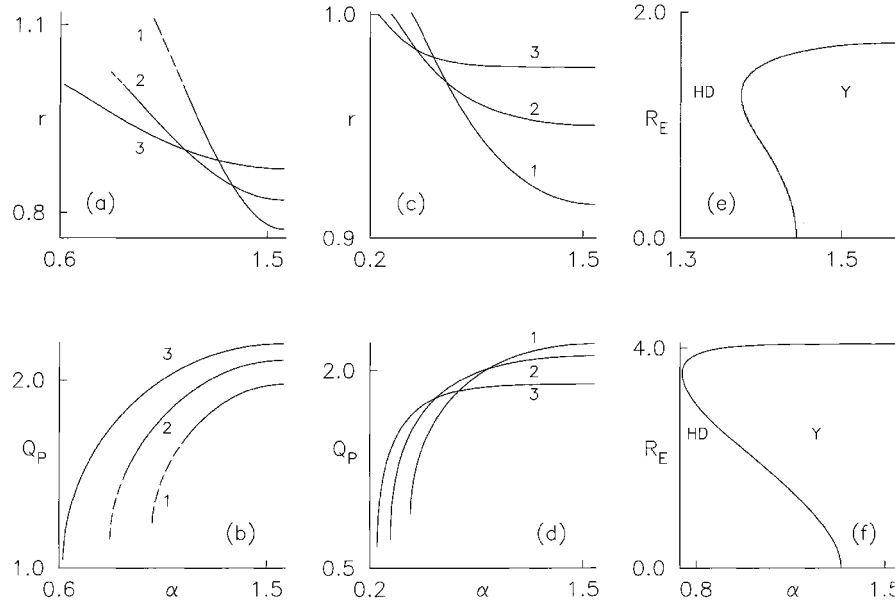

Figure 12. Details as in figure 11 except that the magnetic angle α is varied. In (*a*) and (*b*), $R_E = (1)\ 1$, (2) 2, (3) 3. In (*c*) and (*d*), $R_E = (1)\ 4$, (2) 5, (3) 6. This clearly indicates the shape of the phase boundary between HD and the Y Mode. Phase diagrams are drawn for $k_{12} =$ (*e*) 4, (*f*) 6. Compare with phase boundaries in figure 1 of reference [21] as well as those in figures 8 (*e*) and 8 (*f*) (see also § 6.1).

Flexoelectricity is generally neglected but a qualitative discussion of its possible effect is given in one case. The main conclusions are the following.

Given that $\mathbf{E}_o$ is along x, parallel to $\mathbf{n}_o$; and $\mathbf{H}_\perp$ in the yz plane makes angle α with y; the material is 5CB with ε_A, $\chi_A > 0$. Both PD Modes appear because of destabilizing torques arising from electric perturbations. If $\mathbf{E}_o$ is strong enough, the Y Mode is favourable with $\mathbf{H}_\perp$ acting along z [figures 1 (*a*) and 1 (*b*)]. If $\mathbf{H}_\perp$ is rotated towards y, the X Mode sets in causing a discontinuous change in the periodicity wave vector [figures 1 (*c*), 1 (*d*) and 2)]; further rotation of $\mathbf{H}_\perp$ quenches the X Mode in favour of HD. These effects arise due to an increase in the asymmetry of the perturbations. If $\mathbf{E}_o$ is weak enough, only HD prevails, regardless of the magnetic angle [figure 3 (*a*)]. The results are substantially unchanged for a material with high elastic anisotropy except that the Y Mode now prevails even when $\mathbf{E}_o$ is absent [figures 1 (*a*), 1 (*b*) and 3 (*b*)]; in particular, the Y Mode is never quenched by a strong, stabilizing $\mathbf{E}_o$. Weakening of the azimuthal anchoring encourages the formation of the Y Mode in thin samples (figures 4 and 5); the presence of K_{24} has a similar effect when $\mathbf{E}_o$ is weak (figure 6).

Sections 5 and 6 deal with the Y Mode in high elastic anisotropy materials with $\mathbf{E}_o$ acting along z or y. In both cases, the Y Mode distortions do not perturb $\mathbf{E}_o$. When susceptibility anisotropies are both positive (§ 5.2), the Y Mode induced by $\mathbf{E}_o$ acting along z can be suppressed by a stabilizing $\mathbf{H}_\parallel$ impressed along x (compare figure 7 with figure 1). When susceptibility anisotropies have opposite signs and $\mathbf{H}_\perp$ acts along a symmetry direction, results for the Y Mode can be deduced by simply comparing the forms of governing equations with those of § 5.2 (see § 5.3–§ 5.5). When $\mathbf{H}_\perp$ acts in the yz plane, the phase boundaries between HD and the Y Mode bear remarkable shape similarity in different cases except that the diagrams have to be reflected in a suitable mirror before being brought into qualitative superposition with each other. For example, compare figure 3 (*b*) (curve 1) with figure 10 (*c*) or 10 (*d*); also compare figures 8 (*e*) and 8 (*f*) with figures 12 (*e*) and 12 (*f*).

The results of this work must be interpreted strictly within the framework of the linear perturbation hypothesis which leads to the solution of an eigenvalue problem in every case, so that the actual values of the perturbation amplitudes are not known. Hence, quantitative deduction of post-threshold phenomena is impossible. When a threshold is optically detected, the accompanying deformation is already non-linear. This must be borne in mind while comparing observed threshold parameters with their theoretical counterparts. Some possibilities connected with non-linear effects are discussed below with examples from figures 1 (*a*) and 1 (*b*) of § 3.1.

(i) When the stabilizing $\mathbf{E}_o$ is weak, only the magnetic HD threshold is relevant in 5CB; the X and Y thresholds do not exist. Even if HD appears at the linear threshold, further increase of $H_\perp$ causes HD to develop as a non-linear deformation. The non-linear HD may undergo instability against periodic perturbations when $H_\perp$ is high enough. Such an instability would be analogous to the one studied in [7].

(ii) The true XY Mode linear threshold does not exist in any of the examples studied in this work. The possibility exists, however, that the XY Mode might occur due to the destabilization of one of the other deformations. When $\mathbf{E}_o$ is strong enough, the Y Mode should develop above a magnetic threshold. If $H_\perp$ is raised above the Y threshold, the Y Mode develops into a non-linear distortion which may undergo instability to result in the XY Mode.

(iii) As per equation (10), 5CB has $\chi_A > 0$ and the stable orientation of $\mathbf{n}$ is one parallel to $\mathbf{H}_\perp$. Even if a stabilizing $\mathbf{E}_o$ acts, it is possible that $\mathbf{n}$ in a large portion of the sample will align along $\mathbf{H}_\perp$ if $H_\perp$ is high enough. Suppose the Y Mode develops at the Y threshold. Increase of $H_\perp$ to a high value should cause alignment of $\mathbf{n}$ by $\mathbf{H}_\perp$ leading to a disappearance of the stripes. This non-linear effect has been observed in a nematic having high elastic anisotropy [6], but with $\mathbf{E}_o$ absent.

The thresholds studied in this work describe the change from the undistorted alignment, $\mathbf{n}_o$, to a deformed state. The perturbations imposed are mathematical; the governing equations do not have driving terms which cause the perturbations. These assumptions may be realistic in a thin sample when $\mathbf{E}_o$ acts normal to the plates (§ 5) and the effects of the lateral edges of the sample are insignificant. When $\mathbf{E}_o$ acts in the sample plane, the inter-electrode gap may not be large compared with the sample thickness. Studies on the homeotropic configuration show [31] that a thresholdless distortion develops even in the a.c. case due to thermal fluctuations as well as inhomogeneity in $\mathbf{E}$ (this causes field induced biaxiality [17]). Similar effects may also occur in the planar configuration.

Flexoelectricity has been neglected in this work. This limitation has to be seen in conjunction with the use of only the 'soft' boundary condition for ψ in § 3 and § 4. As flexoelectricity is a polar effect, scaling with respect to sample thickness may not be complete even with the rigid anchoring hypothesis. The mixing of solutions with

pure spatial symmetry caused by flexoelectricity may have considerable influence on the linear thresholds in a thin sample. As indicated earlier (§4.3), the study of PD thresholds in the presence of a d.c. electric field falls outside the scope of this work. The thresholdless HD that develops, as well as its subsequent instability under periodic perturbations, has to be studied along the lines of [19] taking into account electric perturbations. Attempts must also be made to incorporate the full set of boundary conditions for **E**. The nematic is assumed to be an insulator. A real nematic used in an experiment generally has non-zero electrical conductivity whose anisotropy may lead to convective PD [3, 4, 14] and not the static PD studied in this work. Interesting results have been obtained for conducting nematics under the tacit assumption of static equilibrium [9]. As an example, a static PD threshold is shown to exist in a conducting nematic under appropriate assumptions in one configuration (see the Appendix).

Apart from experiments to detect the static PD thresholds, those involving dynamic effects may prove interesting. For instance, the application of a strong destabilizing field is known to lead to a variety of transient periodic dissipative structures [32]. The configuration of §3 and §4 should prove interesting in this regard. Experiments with rotating magnetic fields have led to the discovery of a number of novel patterns in the homeotropic geometry [33]. As shown in §3, the nature of static PD changes when the tilt of $\mathbf{H}_\perp$ is changed in a plane normal to $\mathbf{n}_o$; it should be interesting to investigate the resulting deformation when $\mathbf{H}_\perp$ is rotated with some angular velocity.

The work of [27] concerns nematics with defects confined to cylindrical cavities. PD in uniformly aligned ground states has been theoretically studied [34] with the nematic confined to the annular space between two long coaxial cylinders. The results are similar to those obtained for a flat sample when the ratio of the cylinder radii is close to unity (i.e. when the sample thickness is small compared with the average radius) except that the wave vector (related to the number of domains) may be quantized for some PD Modes. With the invention of techniques to impart specific director alignment on cylindrical surfaces [35], controlled experiments on cylindrical geometry appear feasible. Several results of [20, 21] as well as those of §3 and §4 have theoretical equivalents in cylindrical geometry [36]. The results of §3 can be extended to $\mathbf{n}_o$ and $\mathbf{E}_o$ along x, the cylinder axis, and a radial magnetic field. It appears [36] that PD with azimuthal modulation (analogue of the Y Mode) may set in when the ratio of radii is close to unity. As the sample is closed with respect to the azimuthal variable, the wave vector for azimuthal modulation is quantized. An increase of sample curvature makes the perturbations more asymmetric. Then, PD with x modulation (analogue of the X Mode) appears to be more favourable; this PD Mode has a wave vector that can vary continuously with parameters.

Appendix

We assume that electrical conductivity exists in the rigidly anchored nematic for the configuration of §2 and §3.1 with $\mathbf{E}_o$ acting along x and $\mathbf{H}_\perp$ acting along z ($\alpha = \pi/2$). The principal conductivities are $\Sigma_\parallel$ and $\Sigma_\perp$ with the anisotropy $\Sigma_A = \Sigma_\parallel - \Sigma_\perp$. In the absence of perturbations, the current density $\Sigma_\parallel E_{xo}$ exists along x. Under perturbation, the current density deviates away from x; the torque equations (4) and (5) remain but (3) is not valid as $\operatorname{div}\mathbf{D} = 4\pi\rho$ where ρ is the free charge density. A study of the perturbations in equilibrium is possible by ignoring ρE_{xo}, the body force density along x; this assumption may be valid in some materials if E_{xo} is not very high. Then, equation (3) is replaced by the static limit of the equation of continuity,

$$\Sigma_A E_{xo}(\phi_{,y} + \theta_{,z}) - \Sigma_\parallel \psi_{,xx} - \Sigma_\perp(\psi_{,yy} + \psi_{,zz}) = 0. \tag{A1}$$

As glass is an insulator, the z component of the perturbed current density should vanish [29]. As θ and ϕ also vanish at the boundaries, the condition (9) is recovered.

For the sake of illustration, consider the X Mode. Following the procedure of §3.1, the neutral stability curve for SOLUTION 1 is found to be given by equation (12) with the redefinitions

$$\beta_1 = \frac{\Sigma_\parallel}{\Sigma_\perp}; \quad \omega_E = \frac{\varepsilon_A \Sigma_\parallel E_{xo}^2 h^2}{4\pi K_1 \Sigma_\perp}. \tag{A2}$$

When Q_x vanishes, one recovers the expression for H_F (11) with the new definition for ω_E. The X Mode is found to exist as a solution with threshold lower than that of HD only if

$$E_{xo} > E_3; \quad E_3^2 = \frac{\pi^3 K_3 \Sigma_\perp^2}{h^2 \Sigma_\parallel \Sigma_A \varepsilon_A}. \tag{A3}$$

A necessary condition for E_3 (and also the X Mode) to exist is that $\varepsilon_A \Sigma_A > 0$. The reduced electric field is now defined as $R_E = E_{xo}/E_3$. Computation is done by choosing an appropriate value for $\Sigma_\parallel/\Sigma_\perp$. The solution for the Y Mode proceeds as in §3.1; the Y Mode is found to be uniformly more favourable than the X Mode for $\mathbf{H}_\perp$ directed along z. The variation of threshold parameters with R_E and α, as well as the phase boundaries, are very similar to those contained in figures 1–3. With decrease of α from $\pi/2$, the wave vector changes discontinuously from y modulation to x modulation; when α is low enough, the X Mode also becomes quenched and only HD exists.

References

[1] De Gennes, P. G., and Prost, J., 1993, *The Physics of Liquid Crystals* (Oxford: Oxford University Press).

[2] Chandrasekhar, S., 1992, *Liquid Crystals* (Cambridge: Cambridge University Press).

[3] Blinov, L. M., and Chigrinov, V. G., 1993, *Electrooptic Effects in Liquid Crystal Materials* (New York: Springer).

[4] Pikin, S. A., 1991, *Structural Transformations in Liquid Crystals* (New York: Gordon and Breach).

[5] Rapini, A., and Papoular, M., 1969, *J. Phys. Colloq. Fr.*, **30,** C4-54; for reviews on interfacial properties, see Cognard, J., 1982, *Mol. Cryst. liq. Cryst. Suppl.*, **1,** 1, and Jerome, B., 1991, *Rep. Progr. Phys.*, **54,** 391.

[6] Lonberg, F., and Meyer, R. B., 1985, *Phys. Rev. Lett.*, **55,** 718; Srajer, G., Longberg, F., and Meyer, R. B., 1991, *Phys. Rev. Lett.*, **67,** 1102.

[7] Gooden, C., Mahmood, R., Brisbin, A., Baldwin, A., Johnson, D. L., and Neubert, M. E., 1985, *Phys. Rev. Lett.*, **54,** 1035.

[8] Kini, U. D., 1986, *J. Phys. Fr.*, **47,** 693; Zimmermann, W., and Kramer, L., 1986, *Phys. Rev. Lett.*, **56**, 2655. Oldano, C., 1986, *Phys. Rev. Lett.*, **56,** 1098; Miraldi, E., Oldano, C., and Strigazzi, A., 1986, *Phys. Rev. A*, **34,** 4348; Allender, D. W., Hornreich, R. M., and Johnson, D. L., 1987, *Phys. Rev. Lett.*, **59,** 2654; Kini, U. D., 1990, *Liq. Cryst.*, **7,** 185.

[9] Deuling, H. J., 1978, *Solid State Phys. Suppl.*, **14,** 77; Dozov, I., Barbero, G., Palierne, J. F., and Durand, G., 1986, *Europhys. Lett.*, **1,** 563.

[10] Meyer, R. B., 1968, *Phys. Rev. Lett.*, **22,** 918; Prost, J., and Marcerou, J. P., 1977, *J. Phys. Fr.*, **38,** 315; Durand, G., 1984, *Mol. Cryst. liq. Cryst.*, **113,** 237.

[11] Vistin, L. K., 1970, *Sov. Phys. Crystallogr.*, **15,** 514; Bobylev, Yu. P., Chigrinov, V. G., and Pikin, S. A., 1979, *J. Phys. Colloq. Fr.*, **40,** C3-331.

[12] De Jeu, W. H., Gerritsma, C. J., Van Zanten, P., and Goossens, W. J. A., 1972, *Phys. Lett.*, **39A,** 335; Barnik, M. I., Blinov, L. M., Trufanov, A. N., Chigrinov, V. G., and Korishko, T. V., 1984, *Zh. Eksper, Teor. Fiz.*, **87,** 196.

[13] Derzhanski, A., Petrov, A. G., and Mitov, M. D., 1978, *J. Phys., Paris*, **39,** 273.

[14] A recent review of this subject is Bodenschatz, E., Zimmermann, W., and Kramer, L., 1989, *J. Physique*, **49,** 1875.

[15] Schmidt, D., Schadt, M., and Helfrich, W., 1972, *Z. Naturforsch*, **A27,** 277.

[16] Arakelyan, S. M., Karayan, A. S., and Chilingaryan, Y. S., 1984, *Sov. Phys. Dokl.*, **29,** 202.

[17] Frisken, B. J., and Palffy-Muhoray, P., 1989, *Phys. Rev. A*, **39,** 1513; Frisken, B. J., and Palffy-Muhoray, P., *Phys. Rev. A*, **40,** 6099; Frisken, B. J., and Palffy-Muhoray, P., *Liq. Cryst.*, **5,** 623.

[18] Cummins, P. G., Dunmur, D. A., and Laidler, D. A., 1975, *Mol. Cryst. Liq. Cryst.*, **30,** 109; Bunning, J. D., Faber, T. E., and Sherrell, P. L., 1981, *J. Physique*, **42,** 1175; Sherrell, P. L., and Crellin, D. A., 1979, *J. Physique Colloq. C3, suppl. no. 4*, **40,** C3-211.

[19] Allender, D. W., Frisken, B. J., and Palffy-Muhoray, P., 1989, *Liq. Cryst.*, **5,** 735.

[20] Kini, U. D., 1990, *J. Phys. Fr.*, **51,** 529.

[21] Kini, U. D., 1995, *J. Phys. Fr., II*, **5,** 1841.

[22] Schad, Hp, and Kelly, S. M., 1986, *Mol. Cryst. Liq. Cryst.*, **133,** 75.

[23] Schad, Hp, and Osman, M. A., 1981, *J. Chem. Phys.*, **75,** 880.

[24] Kini, U. D., 1996, *Mol. Cryst. Liq. Cryst.*, **289,** 181.

[25] Kini, U. D., 1996, *Liq. Cryst.*, **21,** 713.

[26] Drzaic, P. S., 1995, *Liquid Crystal Dispersions* (Singapore: World Scientific).

[27] Crawford, G. P., Ondris-Crawford, R. J., Doane, J. W., and Zumer, S., 1996, *Phys. Rev. E*, **53,** 3647 and references therein.

[28] Sparavigna, A., and Strigazzi, A., 1994, *Mol. Cryst. Liq. Cryst.*, **254,** 209.

[29] Landau, L. D., and Lifshitz, E. M., 1984, *Electrodynamics of Continuous Media* (Oxford: Pergamon Press).

[30] Cohen, G., and Hornreich, R. M., 1990, *Phys. Rev. A*, **41,** 4402.

[31] Garg, S., Saeed, S., Wild, S., Bramley, E., and Kini, U. D., 1996, *Mol. Cryst. Liq. Cryst.* (in press).

[32] For a recent review, see Srager, G., Fraden, S., and Meyer, R. B., 1989, *Phys. Rev. A*, **39,** 4828.

[33] Recent work in this area is reported in Migler, K. B., and Meyer, R. B., 1994, *Physica D*, **71,** 412; Frischt, T., and Gilli, J. M., 1995, *J. Phys. Fr. II*, **5,** 561.

[34] Kini, U. D., 1988, *J. Phys. Fr.*, **49,** 527.

[35] Chen, J., Johnson, D. L., Bos, P. J., Sprunt, S., Lando, J., and Mann, Jr, J. A., 1996, *Appl. Phys. Lett.*, **68,** 885.

[36] Kini, U. D. (unpublished).